JOURNAL OF GEOPHYSICAL RESEARCH, VOL. 105, NO. A2, PAGES 2563–2587, FEBRUARY 1, 2000

The geopause in relation to the plasma sheet and the low-latitude boundary layer: Comparison between Wind observations and multifluid simulations

Q. Li, R. M. Winglee, M. Wilber, L. Chen, and G. Parks

Geophysics Program, University of Washington, Seattle

Abstract. Wind observations during the May 10, 1996 perigee are used in conjunction with multifluid global simulations to investigate the mixing of magnetosheath-like plasma and ionospheric plasma in the dawn current sheet. Magnetosheath-like plasma can play important roles in the formation of the low-latitude boundary layer (LLBL) and the cold, dense plasma sheet (CDPS) identified previously in Geotail studies where the magnetosheath component is seen as a low energy component. The Wind observations show that this cold component can be seen well inside the nominal position of the magnetopause and even the CDPS, and is most pronounced near the magnetic equator. This cold plasma provides an important tracer for the geopause where the dynamics of the region inside the boundary is controlled by ionospheric plasma and the region outside is dominated by plasma of solar wind origin. The geopause position in the present case appears be about halfway between the noon-midnight meridian and the magnetopause. In addition, it is shown that the cold magnetosheath-like plasma has significant asymmetries between the northern and southern sides of the current sheet with enhanced cold plasma being observed in the Northern Hemisphere relative to that seen in the Southern Hemisphere. This asymmetry which is also seen in the modeling and is associated with the high dipole ($> 20°$) tilt during the event which allows enhanced entry of magnetosheath plasma in the Northern (summer) Hemisphere and enhanced ionospheric plasma outflows in the Southern (winter) Hemisphere. Flow asymmetries in the particle distributions that have properties similar to the magnetosheath boundary layer are also observed. However, the characteristics of the distributions indicate that the flow is between the LLBL and the CDPS as opposed to the LLBL and the magnetosheath.

1. Introduction

Crossings of the magnetopause show that the region is characterized by multilayered structures [*Paschmann et al.*, 1979; *Sckopke et al.*, 1981]. For southward interplanetary magnetic field (IMF) the structure of the subsolar magnetopause appears to be consistent with that seen in reconnection models as magnetosheath and magnetospheric particles enter the reconnection site from opposite sides and are accelerated along the magnetopause current sheet [*Paschmann*, 1997, and references therein].

For northward IMF, *Song et al.* [1990] have shown that the subsolar magnetopause (as identified by the current layer there) is associated on occasions with two distinct boundary layers. The outer boundary identified by *Song et al.* [1990] is closest to the magnetopause and is composed mostly of magnetosheath-like plasma with a reduced but nonzero component of magnetospheric-like plasma. The ratio of the ion to electron temperature is substantially elevated over that seen in the magnetosheath or in the magnetosphere. In the inner boundary the density of the magnetosheath-like population is substantially smaller, but still of sufficient magnitude that it provides much of the density (of a few particles per cm^3) but the temperature of the plasma is high and magnetospheric-like plasma predominates. These plasma structures have been attributed to reconnection at high latitudes [*Song et al.*], 1993.

Fuselier et al. [1997], using Active Magnetospheric Particle Tracer Explorers/Charge Composition Explorer (AMPTE/CCE) examined the dayside magnetopause for structures in the electron distributions above energies of 50 eV. They showed two transitions as the magnetopause is crossed inbound. The first, called the magnetosheath boundary layer (MSBL), is associated with one half of the electron population seen in the sheath being replaced by a streaming, heated magnetosheath population. The other half remains unchanged until the second transition, identified as the low-latitude bound-

Paper number 1999JA900369.
0148-0227/00/1999JA900369$09.00

ary layer (LLBL) where it is also replaced by a heated population, resulting in a symmetric distribution. Because of the asymmetry in the electron distribution in the MSBL, the field lines there were thought to be open.

Phan et al. [1997] have shown additional structure near the dusk magnetopause using Wind data. They found that the electron parallel temperature is enhanced across the magnetopause and continues to increase across the LLBL, while the perpendicular temperature of the electrons remains approximately constant. The bulk speed of the plasma in the LLBL near the magnetopause is similar to that in the magnetosheath, and as the spacecraft moves away from the magnetopause the bulk speed decreases in association with decreasing plasma density. *Phan et al.* [1997] used this smooth variation to suggest that diffusive processes play a strong role in the formation and dynamics of the LLBL. The particle distributions, particularly for the electrons, with their symmetric appearance, suggest that the LLBL field lines are closed. These conclusions are similar to those of *Williams et al.* [1985], who used ISEE energetic particles on the dawn and dusk magnetopauses during periods of northward IMF. However, they did note that substantial differences between the dawn and dusk magnetopauses are possible.

Once the magnetosheath plasma crosses the magnetopause, there is strong evidence that it can penetrate deep into the magnetosphere. *Fujimoto et al.* [1998a,b], using Geotail data, have shown that cold, dense stagnant ions of magnetosheath origin can be seen several Earth radii (R_e) from the nominal position of the magnetopause. Quasi-neutrality is provided by electrons, which are presumably of magnetosheath origin but which have experienced significant parallel heating. They noted that the cold, dense plasma is not spatially restricted to a thin layer attached to the magnetopause (LLBL) but permeates a substantial part of the magnetotail. Hence they refer to the region not as the LLBL, but as the cold, dense plasma sheet (CDPS).

The suggestion that the magnetosheath is supplying a significant portion of the plasma observed in the magnetosphere is not new. *Lennartsson* [1987, 1992] has shown from ISEE 1 data that the plasma sheet always has a significant component of He^{2+} ions (indicating a nonnegligible contribution from the solar wind source). This population was observed to be the largest during periods of extremely weak geomagnetic activity when the interplanetary magnetic field (IMF) was persistently northward.

Recent statistical studies have also shown that the tail density appears to be well correlated with the solar wind density. Such correlations have been seen both by Geotail [*Terasawa et al.*, 1997] and by ISEE [*Borovsky et al.*, 1997]. In both cases the mass loading appears to be strongest when the IMF is northward, when the magnetosphere, paradoxically, is expected to be relatively closed.

However, the ionosphere is also believed to be an important source of plasma to the magnetosphere [*Chappell et al.*, 1987]. The mixing of the plasmas from the solar wind and ionosphere has led *Moore* [1991] and *Moore and Delcourt* [1995] to propose that within the magnetosphere there is a boundary called the geopause, where the dynamics interior to this boundary is dominated by ionospheric plasma, and the dynamics in regions outside this boundary is dominated by plasma of solar wind origin. The geopause was envisaged to extend into at least the midtail region, as suggested by single-particle tracking [*Delcourt et al.*, 1989, 1993].

More recently, multifluid simulations that separately track the dynamics of the ionospheric and solar wind plasmas [*Winglee*, 1998a,b] have demonstrated that the geopause is a physically important region within the magnetosphere and can be used to identify the characteristics of different regions within the magnetosphere, including the plasma sheet and LLBL. The geopause was shown to be highly dependent on the IMF conditions, with the solar wind being the dominant source of plasma for northward IMF, but during southward IMF the geopause was seen to increase in both extent across the tail and down the length of the tail. In addition, the region where the ionospheric plasma supplied the bulk of the plasma pressure (i.e., the hot plasma) could extend well beyond the density geopause. While the geopause can extend into the midtail region, it appears to be restricted in y, particularly for northward IMF, which would be consistent with the observations described above that note that the sheath appears to be the dominant source of plasma to the LLBL.

In this paper we investigate the structure of the LLBL, and the CDPS, and their extensions into the plasma sheet as seen during a Wind perigee pass that occurred on May 10, 1996. This pass is particularly advantageous for this study because there were several small pressure pulses ($\Delta P < 1$ nPa) in the solar wind which appear to cause the current sheet to shift of the order of 1-2 R_e. As a result, Wind makes several crossings of the current sheet during a 5 hour period. These crossings then provide sampling of the plasma conditions at the center of the current sheet as a function of axial distance from the magnetopause, and allow the identification of the geopause.

It is shown that the Wind data allow the identification of a cold, dense plasma component within the plasma sheet population that is probably of magnetosheath origin and which can extend deep into the magnetosphere. This penetration of cold plasma is also seen in the global simulations of the event and arises from high-latitude reconnection that loads terrestrial field lines with low-energy magnetosheath plasma so that the subsequent convection of the field lines into the magnetosphere leads to the deep penetration of cold plasma. In contrast, the energetic particles observed by Wind are shown to be anticorrelated with

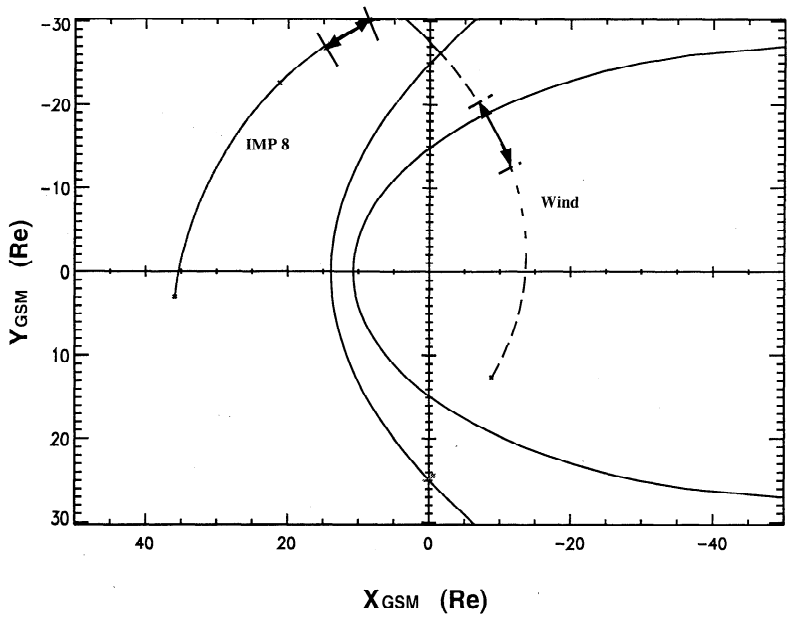

Figure 1. The position of Wind during the May 10, 1996, perigee pass. The solar wind parameters for the event were provided by IMP 8, which was also on the dawnside for the event.

the cold, dense component, and this fact suggests that the two components have different origins or that there are substantial changes in the energy characteristics of the magnetosheath as it circulates around the magnetosphere. In the global modeling, the anticorrelation between the cold, dense component and the energetic component is produced by the mixing of ionospheric and magnetosheath plasma. The energetic component is associated with outflowing ionospheric plasma which experiences stronger adiabatic heating as it is convected in z into the current sheet, so that the source of the more energetic particles lies near the noon-night meridian.

2. Instrument

Data for this study were obtained from the Wind spacecraft. The three-dimensional plasma and energetic particle (3DP) experiment is a collection of plasma and energetic particle detectors. Among them, four solid state telescopes (SSTs) are used to detect the energetic particles (60 keV to 7 MeV ions and 26 - 519 keV electrons), while another group of four electrostatic analyzers (ESA's) record particles of low and intermediate energies. The data from these latter instruments are the focus of this paper.

The electrons are measured by EESA-L and EESA-H which cover the energy ranges (with overlapping bins) from 8 eV to 1.1 keV and 30 eV to 27 keV, respectively. The ions are sampled by PESA-L and PESA-H. PESA-L was designed to measure the solar wind protons, which are characterized by a narrow range of velocities. Interior of the bow shock, PESA-H provides the more comprehensive ion measurements due to the distribution of energy bins. The energy range covered by PESA-H is between 80 eV and 27 keV.

All of the ESAs have very high intrinsic geometry factors (10^{-2}cm^2 sr eV for protons and 10^{-1}cm^2 sr eV for electrons), which are up to 2 orders of magnitude higher than those on board earlier-generation satellites. In order to prevent saturation by the cold solar wind core, EESA-L and PESA-L have mechanical attenuators that reduce their geometry factors by about two orders of magnitude. A full three-dimensional (3-D) distribution is obtained every spin period (3 s); however, because of telemetry limitations, the distributions are averaged on board over several spins before being telemetered to the ground. On May 10, 1996, the time resolutions are 51 s for PESA, while for EESA, 3 s distributions are sent down every 26 s. More details about Wind 3DP instrumentation are given by *Lin et al.* [1995]. The Magnetic Field Investigate (MFI) packet on Wind can detect three component magnetic fields. The accuracy of the MFI magnetometers is about 0.080 nT. The magnetic field data used here is averaged over 3 s [*Lepping et al.*, 1995], which is comparable to the EESA integration period. Solar wind conditions, including plasma density, velocity and IMF, were obtained from data from IMP-8 which was on the sunward side of the dawn bow shock at about $y \approx 20R_e$.

3. Overview of Observations

The data in this paper were obtained during a perigee crossing of Wind at the dawnside flank of magnetopause on May 10, 1996. An interval of 6 hours (1700 - 2300 UT) is studied, during which Wind made several cross-

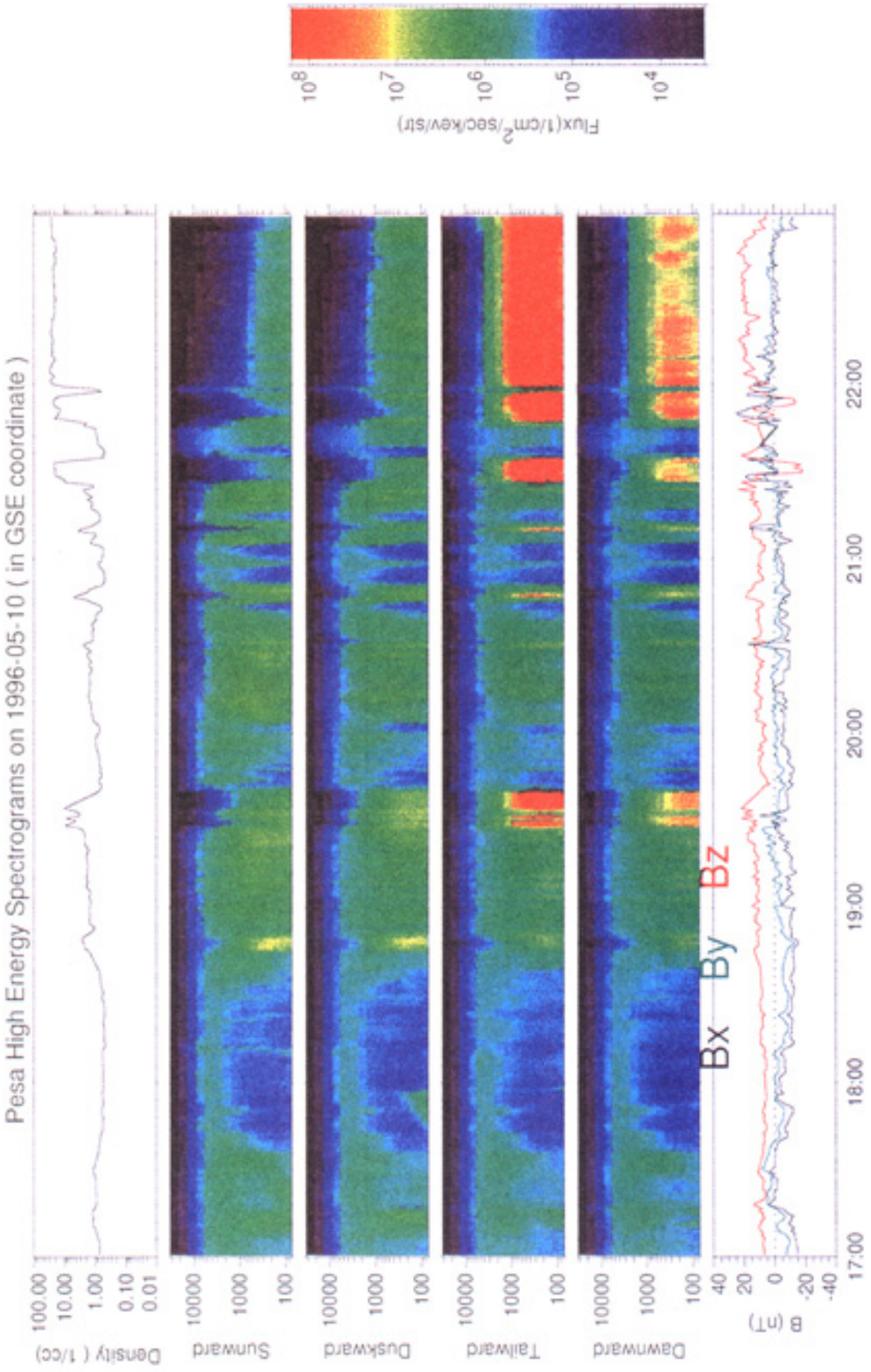

Plate 1. Ion energy spectrograms from PESA-H subdivided into sunward, duskward, tailward, and dawnward components. The magnetopause crossing occurred at 2200 UT. A low-energy component was seen through much of the Wind perigee pass, and its energy characteristics were similar to the magnetosheath component, albeit at lower densities.

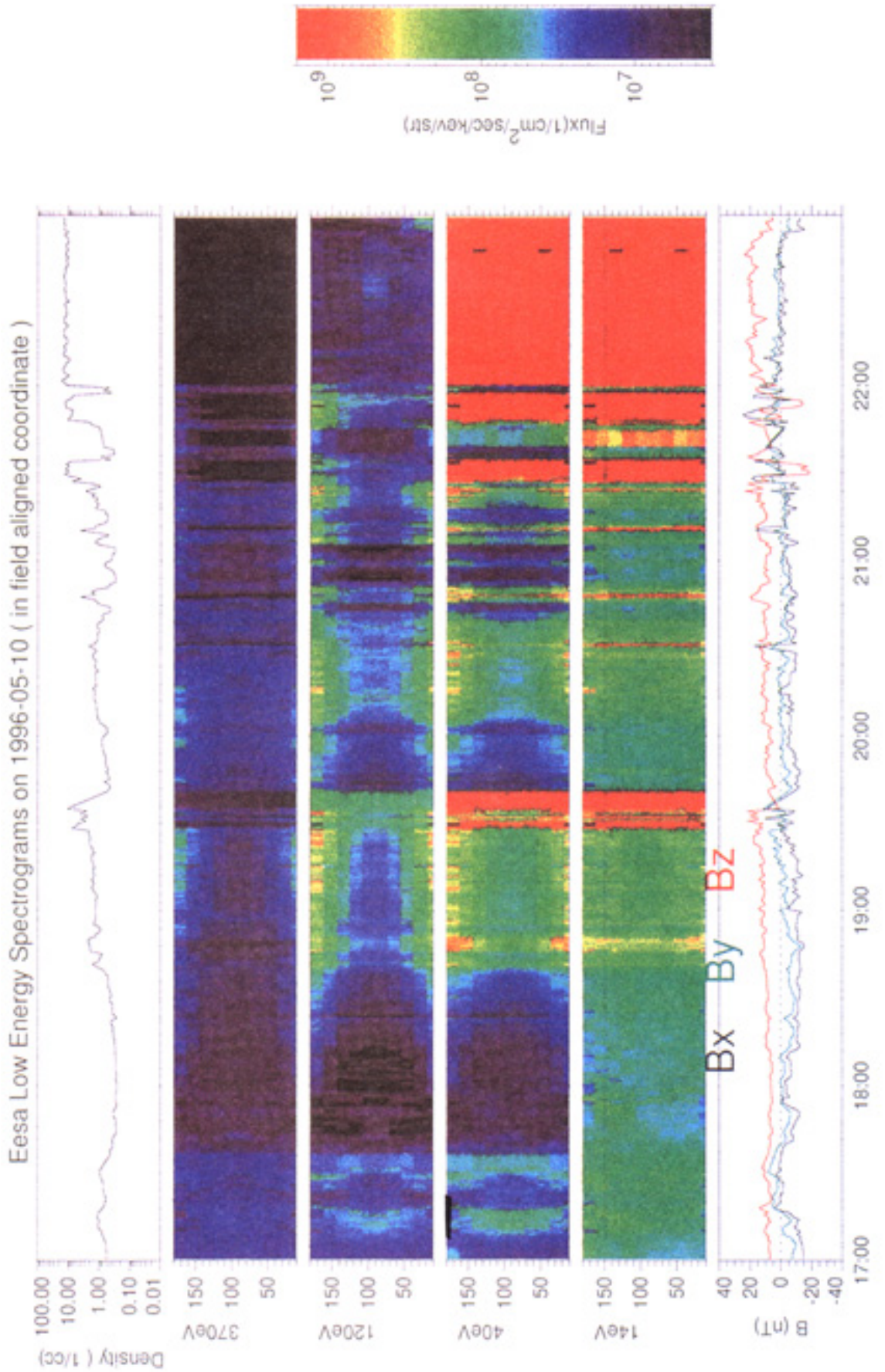

Plate 2. The top spectrograms show the electron density derived from EESA-L for electrons with energies 14 eV and above. The middle spectrograms show pitch angle of electrons at 14, 40, 120, and 370 eV. The bottom graph shows the magnetic field data for timing purposes. The entry of dense cold plasma can be seen at 1935, 2130, and 2155 UT. The incursions are accompanied by higher-energy components (e.g., at 120 eV) which are very much weaker than in the magnetosheath, indicating that the magnetopause was not crossed. The electrons in the cold, dense plasma sheet (CDPS) are seen to have a strong field-aligned component over a broad range of energies.

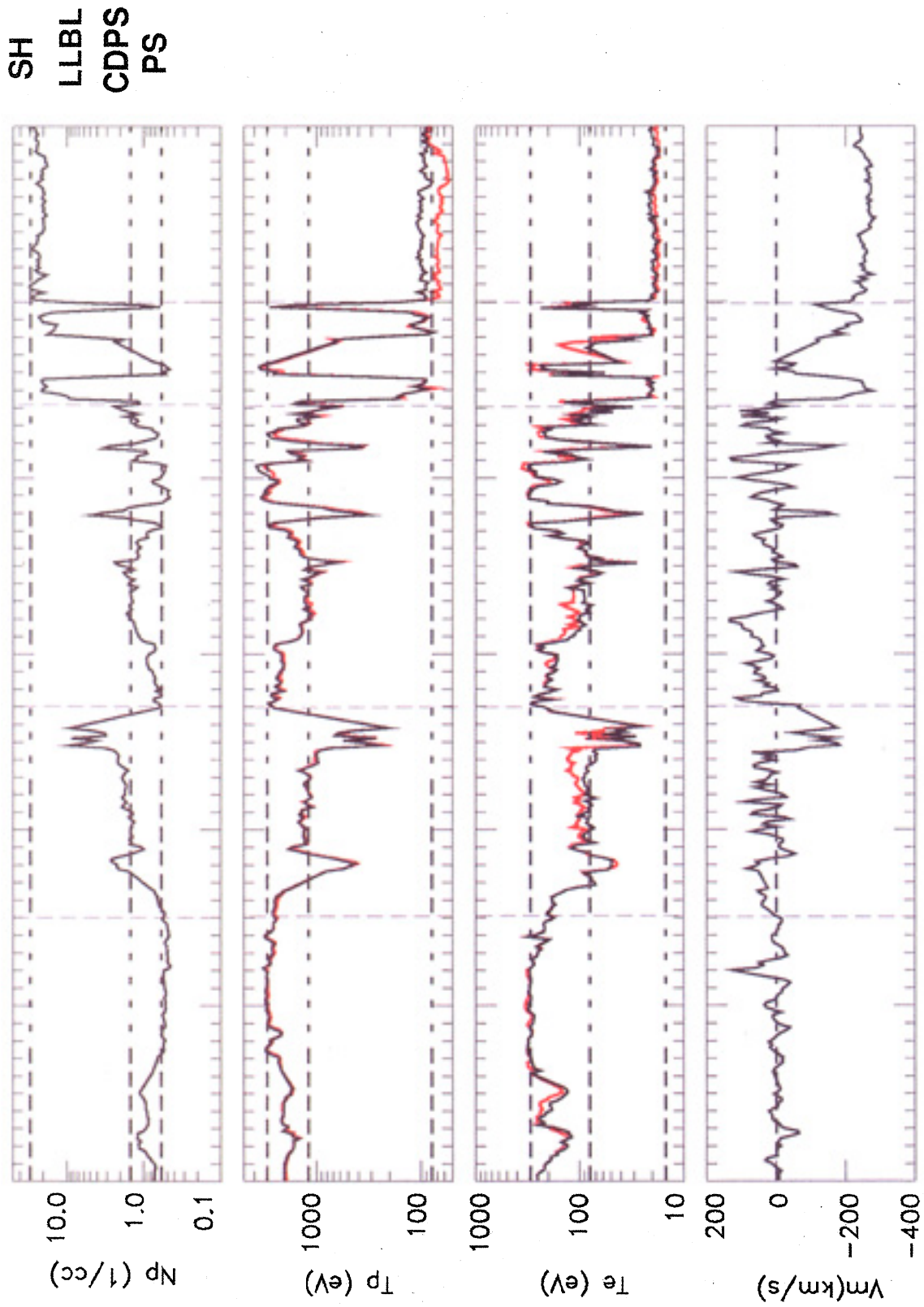

Plate 3. Bulk characteristics of the plasma during the event. These bulk parameters are suggestive of four distinct regions, the plasma sheet (PS), the cold, dense plasma sheet (CDPS), the low-latitude boundary layer (LLBL), and the magnetosheath (SH). In the middle graphs, the perpendicular (parallel) temperatures are indicated by the black (red) lines.

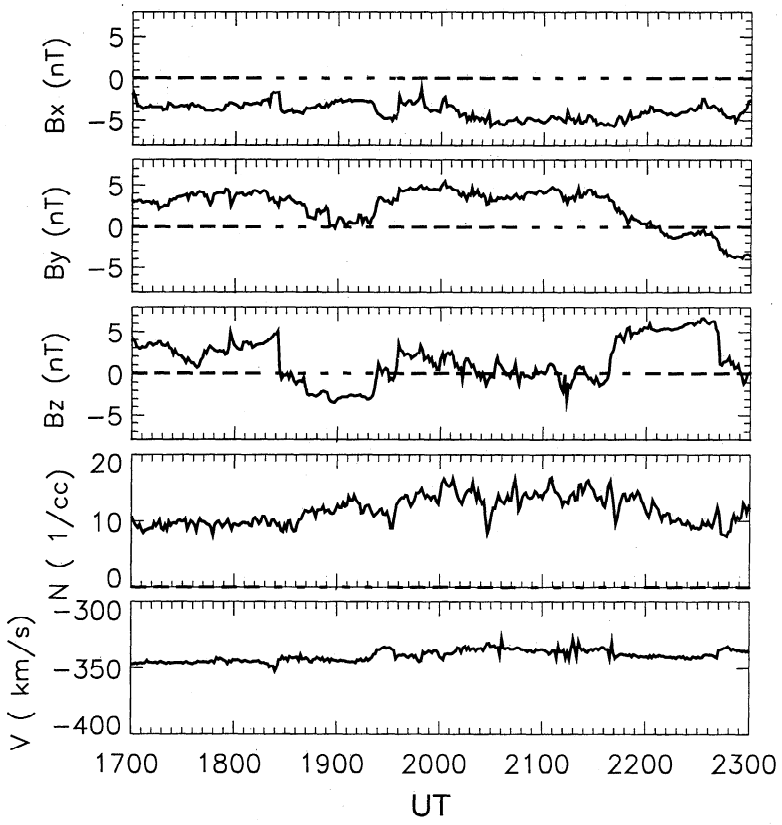

Figure 2. The solar wind conditions as observed by IMP 8. Interplanetary magnetic field (IMF) B_x and B_y were approximately constant for the event, while IMF B_z was initially strongly northward at about 5 nT for the first 1.5 hours, followed by a 50 min period of southward (-2 nT) IMF, and then remained on average near zero until about 20 min prior to the Wind magnetopause crossing at 2200 UT. At this time it turned strongly northward. The solar wind density was approximately steady for the first 1.5 hours, in association with the period of strong northward IMF. The density then on average increased by about 50% over the next 3 hours, but the increase was not monotonic.

ings through the dawn plasma sheet. The position of Wind during the interval is shown in Figure 1 relative to the nominal positions of the bow shock and magnetopause. At 1700 UT, Wind was inside the magnetosphere at (x,y,z) = (-12,-12,-2) R_e (GSM) and crossed the magnetopause at about 2200 UT at (-8, -17,-6) R_e. The dipole tilt for this period was fairly high, ranging from about 29° to 19°. This large tilt will be important later in explaining some of the asymmetries seen between the Northern and Southern Hemispheres.

The solar wind parameters for the event were provided by IMP 8 and are shown in Figure 2. IMP was a few R_E sunward of the dawn bow shock at $y \sim -30$ R_E. The x component of the IMF was primarily in the antisunward direction, while IMF B_y was primarily in the dusk direction. IMF B_z was northward for the period between 1700 and 1824 UT, southward for the next hour, and then near zero until about 20 min before the magnetopause crossing at 2200 UT, when IMF B_z became strongly northward with about 5 nT field strength.

The solar wind speed was approximately constant at about 340 km s^{-1}. The density, on the other hand, was on average increasing from about 9 cm^{-3} to 15 cm^{-3}. However, the increase was not smooth but instead contained several small bursts where the density increased by about 20-50%. At first glance it might be assumed that these pulses are insignificant. Certainly, the nominal position of the magnetopause is not expected to change by more than an R_e for these solar wind conditions [e.g., *Roelof and Sibeck*, 1993; *Elsen and Winglee*, 1997]. However, we will show in the following sections that they are associated with Wind crossing the current sheet and observing a plasma with substantially different bulk properties.

4. Four Regions

The ion data from PESA-H (80 eV to 27 keV) are shown in the energy spectrograms in Plate 1. The data have been split into sunward, duskward, tailward and dawnward components respectively. The magnetosheath crossing at 2200 UT is marked by a period of high ion fluxes moving in the tailward direction at energies of a few keV. The magnetopause is also marked by the perpendicular temperature in both the ions and

electrons increasing above the parallel temperature (see also Plate 3). There are three other times (1930, 2130, and 2150 UT) when high ion fluxes are also seen. These later times can be ruled out as magnetopause crossings based on the specific characteristics of the particle distributions (discussed later), including the fact that they do not show the same jump in perpendicular temperature.

The most striking feature of Plate 1 is that low-energy (< 1 keV) ions are seen almost throughout the entire period. The main times when this low-energy component almost vanishes are 1730 - 1830 UT and around 2055 and 2105 UT. We shall refer to these regions as the "plasma sheet" which is consistent with existing literature but may not be an accurate description of the true nature of the plasma.

The corresponding electron spectrogram from EESA-L is shown in Plate 2. The electron data below about 13 eV contain photoelectrons, particularly when Wind is in the magnetosphere. The data in this energy range are neglected in the following, which means that in calculating densities it is possible that not all the particles have been fully accounted for. It is seen that the high-density ion events at 1930, 2130, and 2150 UT are accompanied by enhanced fluxes of low-energy (< 300 eV) electrons. However, in comparing the characteristics of these electrons with those in the magnetosheath proper, it is seen that these electrons extend well beyond the 100 eV sheath electrons. This feature is one of several which indicates that these high-density regions are not due to multiple crossing of the magnetopause but represent physically distinct regions.

The second feature is that even excluding the high-density regions, large fluxes of low- to moderate- energy (< 40 eV) electrons are seen throughout much of the event. This population lies at intermediate energies between that seen in the magnetosheath (< 100 eV) and that seen in the "plasma sheet" (> 100 eV). These intermediate electrons will be shown to be similar to the electrons identified by *Fujimoto et al.* [1998a,b] as heated magnetosheath electrons.

The bulk parameters corresponding to the data in Plates 1 and 2 are shown in Plate 3. By inspection four distinct regions can be identified: (1) the magnetosheath with a density of 20 - 30 cm^{-3}, a low ion temperature (< 100 eV), a low electron temperature of < 20 eV, and tailward bulk velocity > 200 km s^{-1}; (2) LLBL with an intermediate density (2 - 20 cm^{-3}), intermediate temperature (ions between 100 to 1000 eV) and bulk velocity of 0 - 200 km s^{-1}; (3) CDPS with moderate densities of 0.6 to 2 cm^{-3}, ion temperatures of 1000 to 2000 eV, with significant temperature anisotropies in electron parallel and perpendicular temperatures; and (4) the "plasma sheet" with low density of < 0.6 cm^{-3}, high ion (> 2000 eV) and electron (> 300 eV) temperatures, with little anisotropy in the electron temperatures.

This ordering of regions becomes clearer if the data are plotted as a function of density [cf. *Phan et al.*, 1997] as in Figure 3. These regions closely resemble those seen in other case studies of magnetopause crossings [e.g., *Paschmann et al.*, 1979; *Sckopke et al,*, 1981; *Phan et al.*, 1997; *Fujimoto et al.*, 1998a,b]. An alternative nomenclature might be that the LLBL and CDPS may be equivalent to the outer and inner boundary layers as identified by *Song et al.* [1990, 1993], or the CDPS may be related to the "halo" region identified by *Sckopke et al.,* [1981].

The bulk parameters as ordered by time in Plate 3 might suggest that the four regions are spatially separate regions, while ordering the data with respect to density in Figure 3 suggests that there is a smooth transition between the regions. In the later case, it is plausible to argue that the four regions represent a continuous radial change in conditions as the magnetopause is approached. We argue in the following section that this picture is an oversimplification, and possibly misleading, because it does not take into account variations in height (or z) from the center of the current sheet.

5. Current Sheet Crossings Induced by Pressure Pulses

The origin of the large density enhancements seen in the tail can be identified by comparing the solar wind dynamic pressure as observed by IMP 8 with the magnetic field components as observed by Wind, as shown in Figure 4. We make the standard assumption that if we are inside the magnetopause and B_x vanishes then the center of the tail current has been encountered. The first set of crossings occurs around 1730 UT.

There are an additional six current sheet crossings starting around 1930 UT. Comparison with the solar wind dynamic pressure indicates that each of these six crossings is preceded by a solar wind pulse about 20 min earlier. The fact that the effects from individual pressure pulses can be seen is surprising since the pulses represent only small changes in total pressure (of the order of 1 nPa), but which correspond to a moderate 20 - 50% change in relative amplitude.

Figure 5 correlates the changes in the tail density with the strength of the tail B_x. The densities have been computed for two energy ranges. It is seen that the appearance of the high-density components is due to an increase in low-energy ions, while at the same time the density of the high-energy component decreases. This is also true for electrons (not shown).

Nearly all the high-density regions in Figure 5 are associated with the crossing of the current into the Northern Hemisphere (i.e., B_x going from predominantly negative values to zero on average or positive). The implication is that the Northern Hemisphere, which is tilted toward the Sun, experiences more mass loading from the solar wind than the Southern Hemisphere.

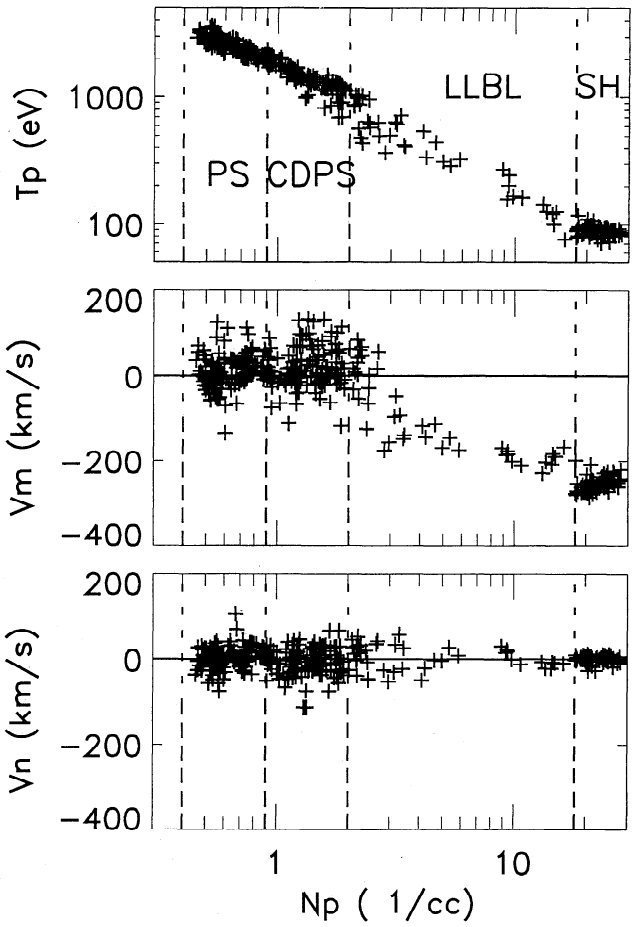

Figure 3. Correlation of bulk parameters with ion density, with V_m being the velocity parallel to the boundary and V_n being the normal velocity. This gives an ordering of the data similar to *Phan et al.* [1997] seen in other magnetopause crossings.

The current sheet crossings provide us with additional key information since they can be used to remove ambiguities associated with z dependences from the center of the current sheet. The bottom panel of Figure 5 shows the variation of density as a function of radial distance for the current sheet crossings (as defined by $\mid B_x \mid < 0.5$ for an average of 51 s, which is the ion integration time). The density has been divided into high-energy (0.4 to 27 keV) and low-energy (0.08 to 0.4 keV) components.

The density of the low-energy component in the vicinity of the center of the current sheet is seen to increase monotonically as the magnetopause is approached. This suggests that this plasma is of magnetosheath origin and that the density variations seen in the data may actually be due to variations in both z and axial distance. Moreover, the large extent of the observations over some 6 R_E can be used to rule out the possibility that they are due to the magnetopause moving back and forth across the spacecraft position; the magnetopause motion for the size of these pressure pulses is expected to be less than 1 R_E.

In contrast, the density of the energetic ions decreases monotonically toward the magnetopause, and hence is anticorrelated with the low-energy magnetosheath-like plasma. These observations suggest that the energetic plasma in the current sheet is either derived from a different source (e.g., of ionospheric origin) or it is magnetosheath plasma which has been accelerated to high energies somewhere within the magnetosphere. In particular, the density profile of the energetic ions suggests a source toward the noon-midnight meridian as opposed to the magnetopause. An ionospheric source for the energetic ions would provide the simplest explanation for a source centered around the noon-midnight meridian. Nevertheless, recirculation of magnetosheath plasma within the magnetosphere cannot be directly ruled out as the source. Both hypotheses can be tested with the simulations in section 7.

6. Relationships Among the Four Regions

The relationships among the different regions can be seen through a study of the particle distributions of the different regions as illustrated in Plate 4. The top row shows examples of the electron distributions as measured by EEAS-H (80 eV to 27 keV), while the second row shows the distributions as measured by EEAS-L (15 eV to 1 keV). The 15 eV lower energy limit is indicated by the black circles in the distribution functions.

The bottom panels shows the ion distributions as measured by PESA-H (80 eV to 27 keV). The 80 eV lower limit is indicated by the black circle. All distributions are shown in the convecting plasma frame, that is, in which the average perpendicular velocity has been subtracted. This frame, as opposed to the plasma frame, is chosen so that the presence of any low-energy component in the magnetosphere would be more easily distinguished from the one count statistics if the plasma has a nonzero flow. In the magnetosheath the flow is primarily perpendicular to the magnetic field so that the convecting frame and the plasma frame are essentially the same. The plus in each of the panels represents the velocity shift between the spacecraft frame and the convecting frame. The time histories of the plasma density and magnetic field are shown in the third row and can be used to identify the time period and bulk parameters of the regions being sampled.

The magnetosheath electrons (2210 UT) are approximately isotropic, while the ions show a perpendicular anisotropy as well as enhanced energetic fluxes in the field-aligned direction. The latter component is due to shock-accelerated particles and/or leakage.

The LLBL ion distribution, similar to the magnetosheath distribution, has a significant low-energy component but differs in that the energetic component now

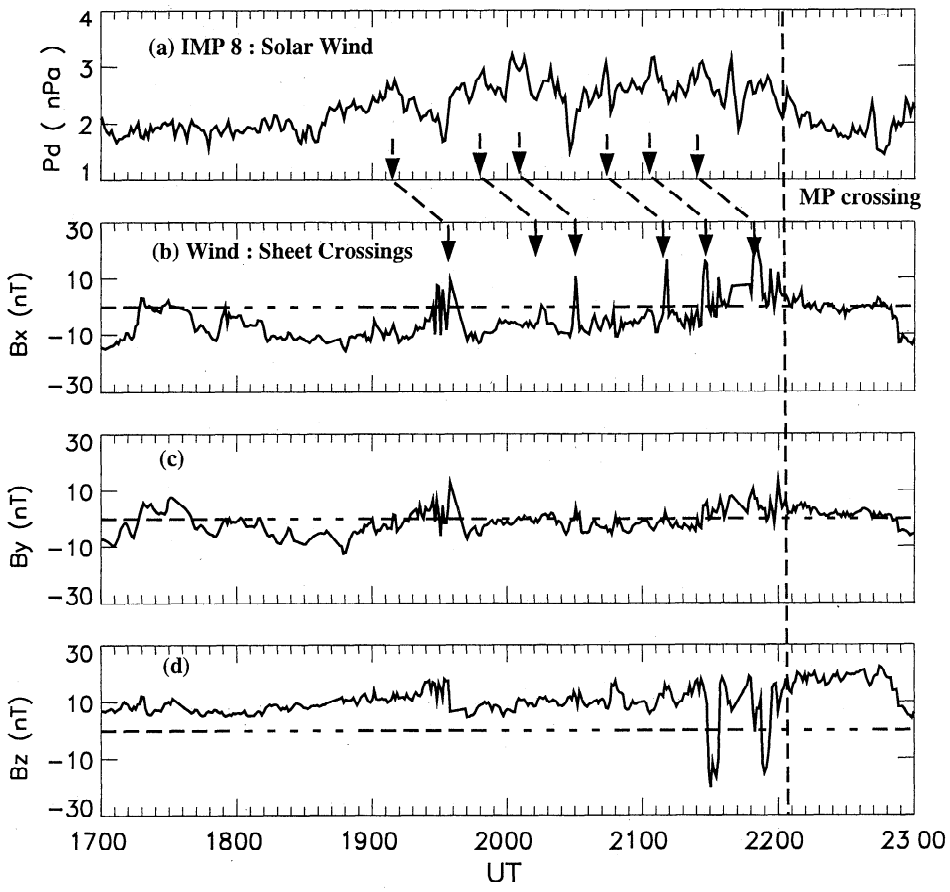

Figure 4. (a)Time history of the solar wind dynamic pressure as observed by IMP 8 and (b-d) the magnetic field components as observed by Wind. It is seen that several of the pressure pulses or local peaks in the dynamic pressure are correlated with Wind's crossing the current sheet from the south and/or moving deeper into the northern side of the current sheet, as evidenced by B_x changing from negative values to zero or to more positive values.

appears more isotropic. The ions have a perpendicular drift to the magnetic field of about 100 km s^{-1}. The electrons show a similar mix of low- and high-energy components, with the low-energy component having a weak parallel temperature anisotropy. Relative to the LLBL, the CDPS ions have a reduced density in the low-energy component, and an increased density in the energetic component. The electrons have a similar trend, but the low energy component has an enhanced parallel temperature anisotropy. This anisotropy is the same as seen by *Fujimoto et al.* [1998a,b] and was interpreted as a marker for the presence of magnetosheath-like plasma.

Moving to the "plasma sheet", the density of the energetic component appears approximately constant, and the electrons extend to even higher energies. However, there are cold magnetosheath-like components in both the ions and electrons that are still evident, albeit at substantially reduced densities relative to the LLBL. As discussed later, the densities of the cold component may appear small due to the z displacement of the spacecraft away from the center of the current sheet and because large densities of cold plasma can still be present near the center of the current sheet.

The changes in the properties of the cold component are illustrated in Plate 5, which compares the distributions from the LLBL regions with those from the magnetosheath. The LLBL distributions closest to the sheath (i.e., at 2150 UT) show substantial flow anisotropies. Flow symmetries are also seen in the ion and electron distributions at 2132 UT, albeit to a weaker extent. The LLBL distributions at 1932 UT are symmetric for the electrons and ions. Thus even though the region has a very high density of nearly 10 cm^{-3}, the data indicate that the region is well away from the magnetopause, since no flow asymmetries are observed. The distributions associated with the other density spikes are also symmetric, indicating that the cold, dense plasma can be seen on possibly closed field lines well inside the magnetopause.

There are two tests that can be made on the particle

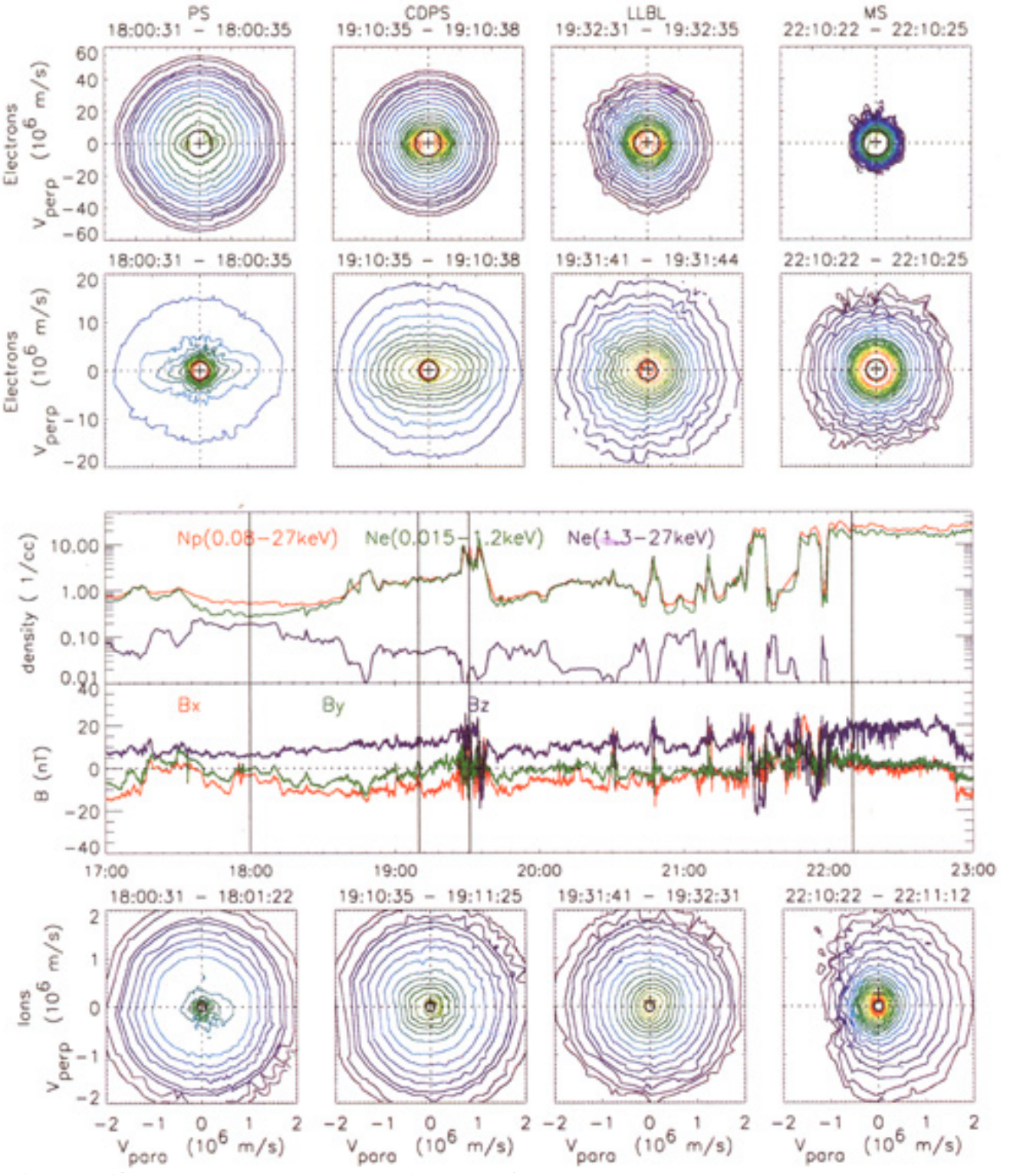

Plate 4. Particle distributions from EESA-H (high-energy electrons; first row), EESA-L (low-energy electrons; second row), and the ions from PESA-H (bottom row). The four regions, PS (1800 UT), CDPS (1910 UT), LLBL (1932 UT), and magnetosheath (2210 UT), identified in the bulk parameters also have very distinct particle distributions.

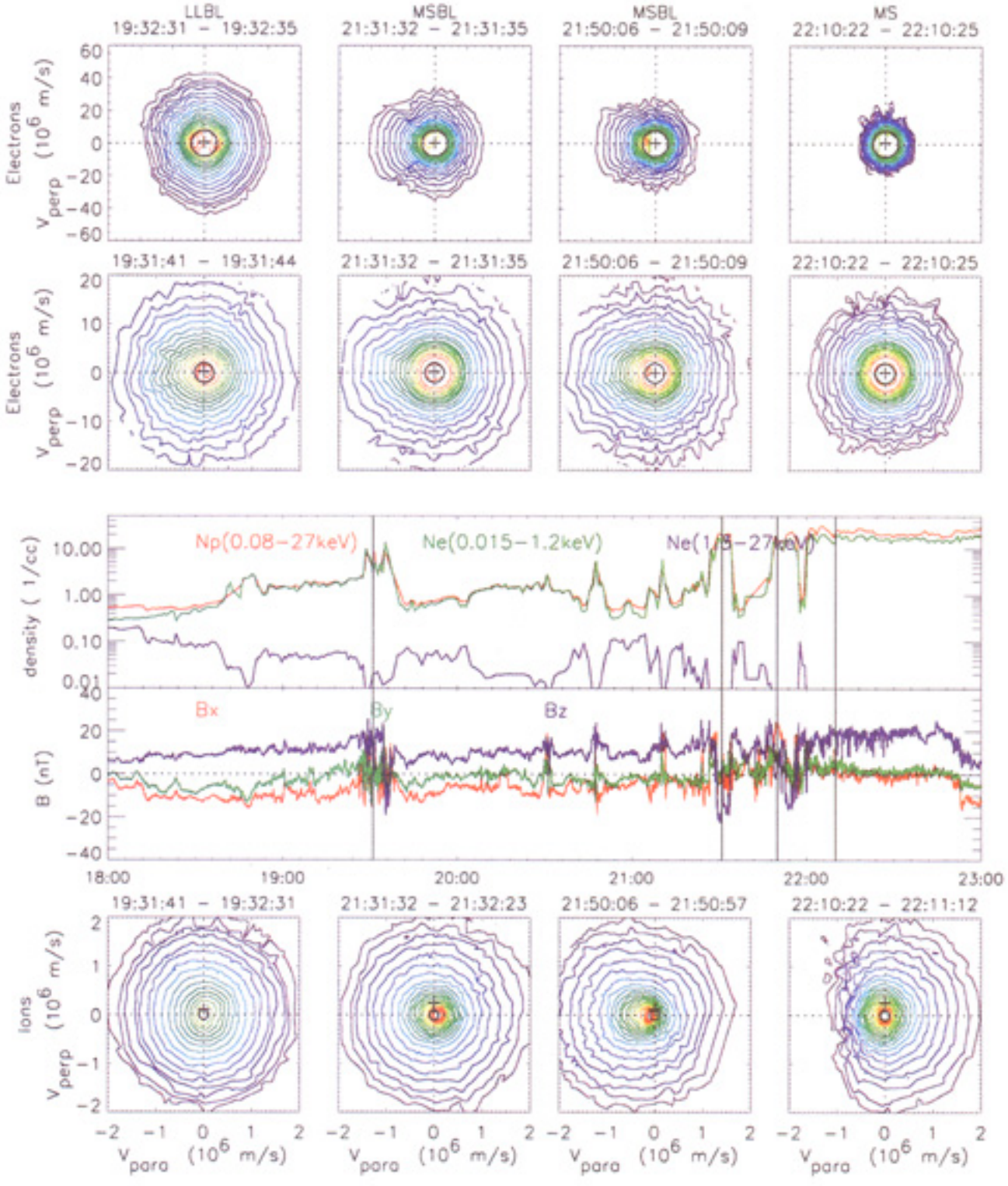

Plate 5. Representative distributions from the four-high density regions seen during the event. The distributions at 2150 UT are asymmetric, which is a characteristic of the MSBL, indicating an open field line. The distribution at 1932 UT does not show this asymmetry, suggesting that field lines are closed and well away from the magnetopause since the MSBL is not encountered.

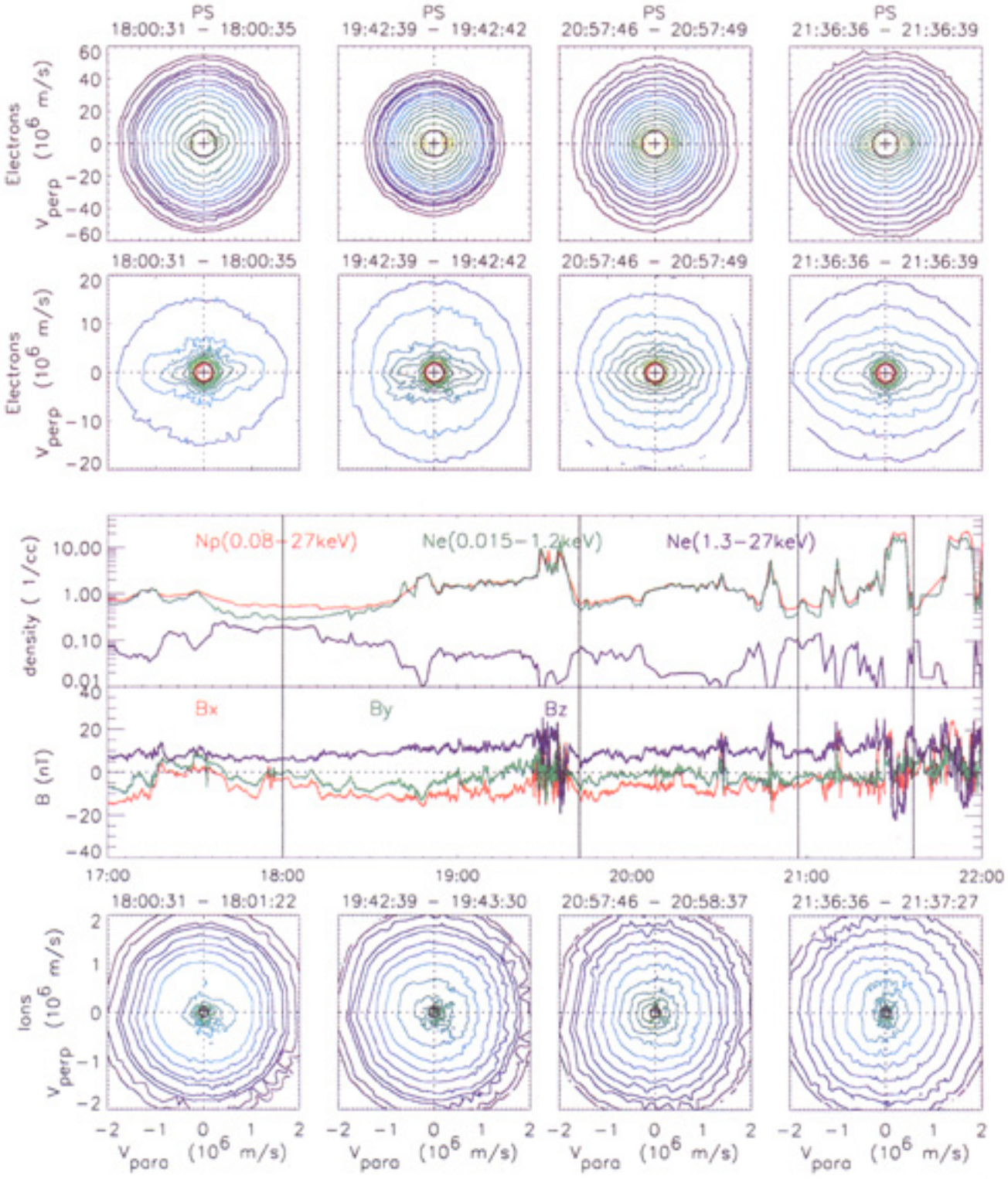

Plate 6. Four distributions from regions identified in the bulk parameters that are representative of the plasma sheet (PS). In all cases the electrons show a low-energy component that has a parallel temperature excess. This population is similar to that seen in the LLBL but at reduced density. Similarly, while the ion distributions are dominated by the energetic component, a cold component is still seen to be present, albeit at reduced densities away from the magnetopause.

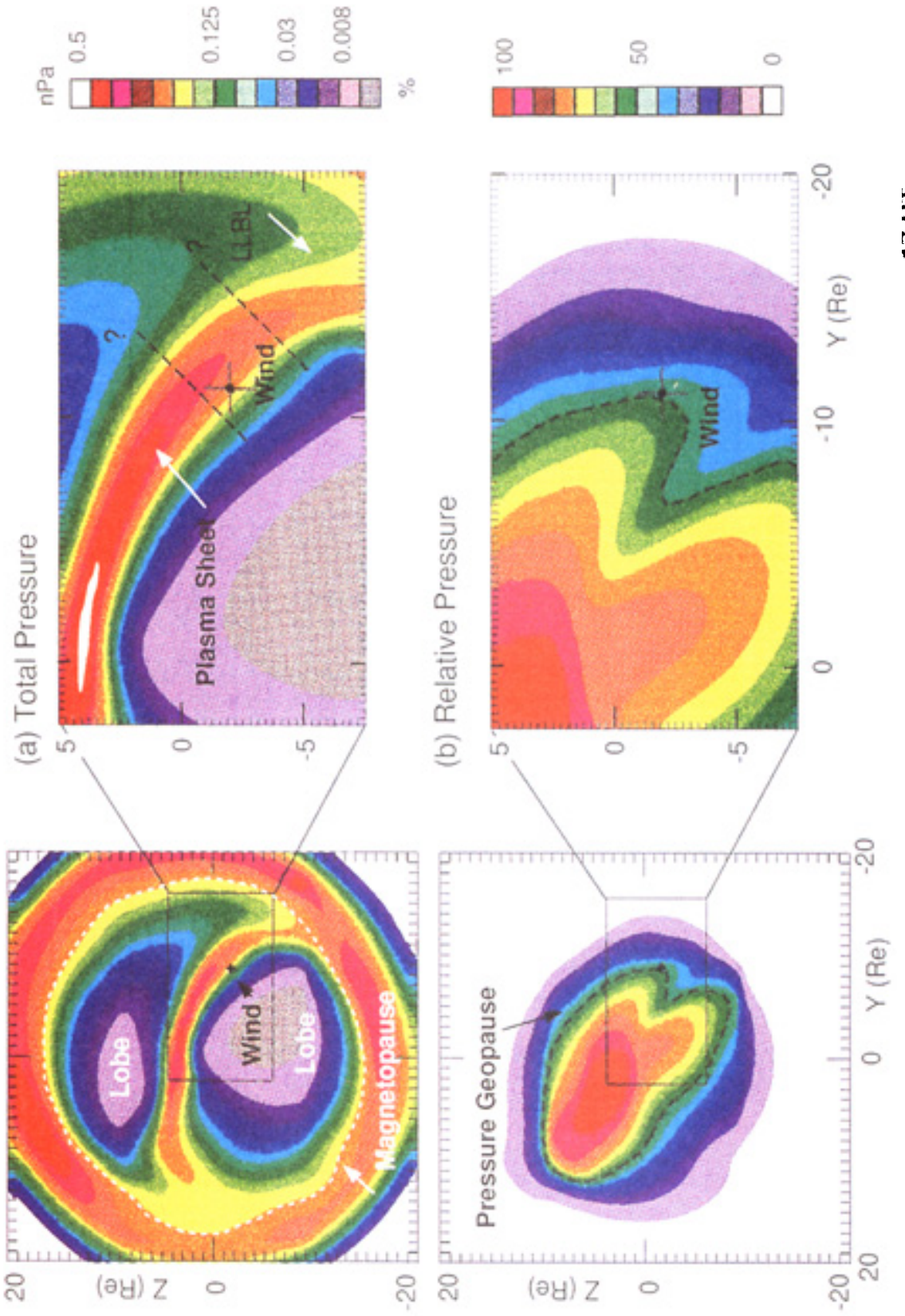

Plate 7. Model results showing the cross-tail configuration at Wind at 1700 UT. Top contours show the total pressure. Bottom contours show the relative plasma pressure with greater than (less than) 50% indicating regions dominated by ionospheric (magnetosheath) plasma. The central reigon is shown on the right hand side at high resolution. At this time in the vicinity of Wind, there are almost equal contributions to the plasma from both sources.

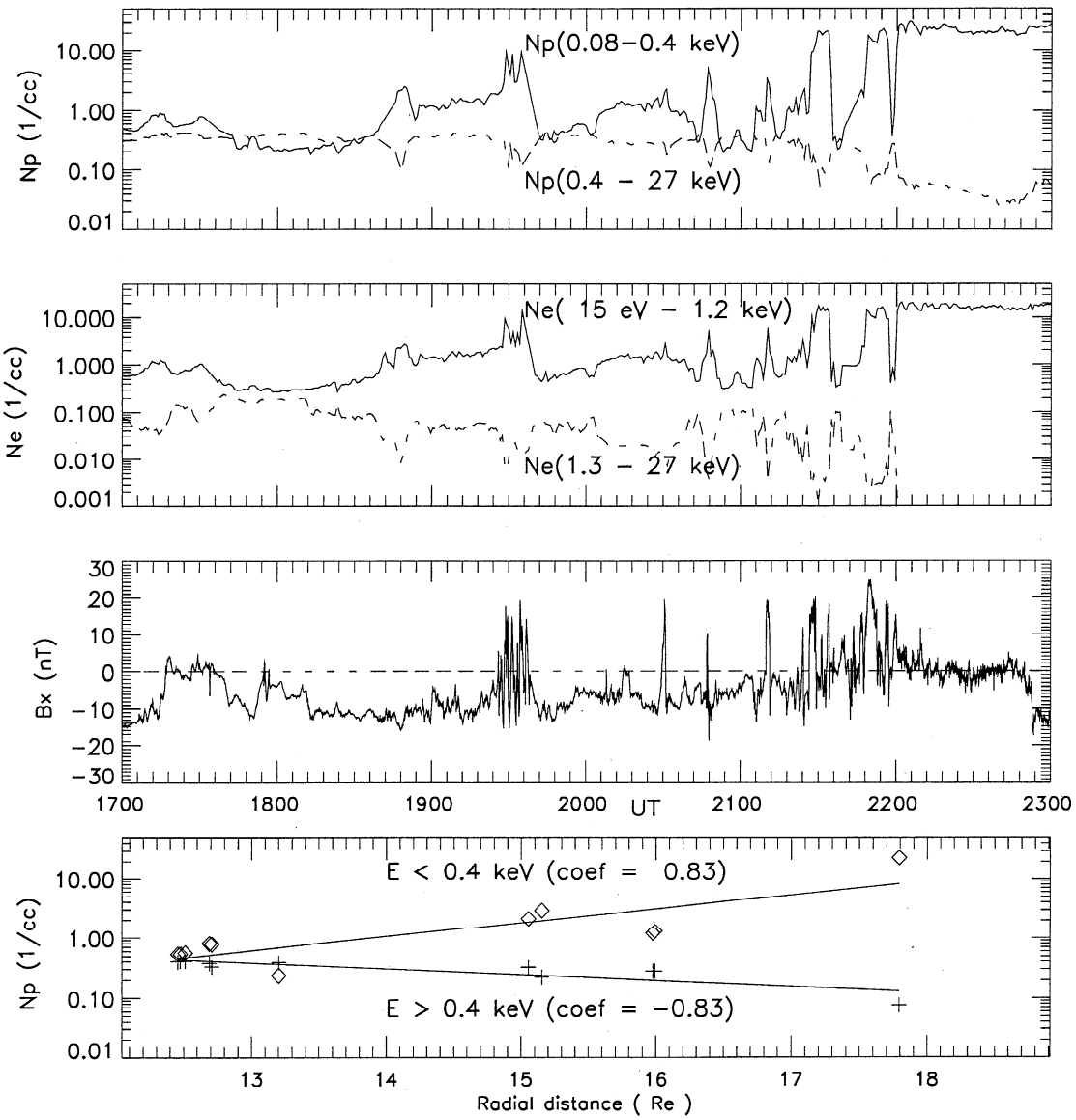

Figure 5. Density of the ions and electrons split into low-energy (solid line) and high-energy components (dashed line). The densities of the two components appear anticorrelated. The density of the low energy component appears well correlated with current sheet crossings ($B_x \sim 0$) or excursions into the northern current sheet ($B_x > 0$). The densities determined from the current sheet crossings are well correlated with radial distance, with the cold and energetic components have opposite slopes, indicating different sources for the two populations and suggesting that much of the observed temporal changes may be due to z variations as opposed to true structures.

distributions to determine whether the cold plasma seen in the above distributions is of magnetosheath origin. First, we tested whether the asymmetric distributions can be reconstructed using distributions from adjacent regions. This test is illustrated in Figure 6 where the top panels show the EEAS-L electron distribution from the LLBL at 2133 UT (Figure 6a) and the cold dense plasma sheet (Figure 6b) at 1910 UT. If one adds the right hand side of Figure 6a to the left hand side of Figure 6b with a ratio of 1 to 0.4, the composite electron distribution of Figure 6c is attained, suggesting possible flow between the two regions. The composite distribution shows many of the features of the observed distribution as displayed in Figure 6d. Similar constructions can be used to account for the ion distributions at this time.

Paradoxically, the distributions with flow asymmetries cannot be reconstructed from a superposition of LLBL and magnetosheath distributions. The magnetosheath distributions do not have sufficient flux of

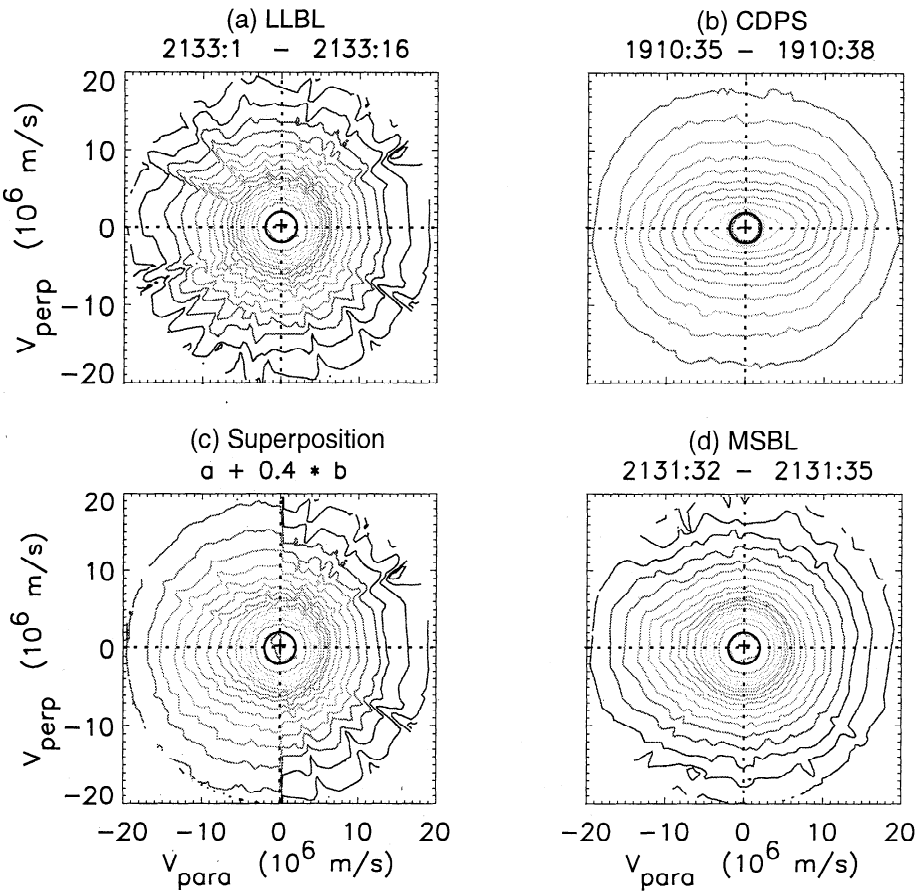

Figure 6. Reconstruction of the asymmetric EESA-L distribution by the superposition LLBL and CDPS particle distributions.

high-energy electrons on the magnetosheath side and the LLBL distributions do not have a sufficient parallel temperature anisotropy to produce the correct form of the flows of the magnetospheric side. Thus while the distributions have many of the properties of the MSBL as identified by *Fusilier et al.* [1997], including the proximity to the magnetopause in the time history, the present results are consistent with an open field line that passes through the CDPS and LLBL and eventually to the magnetopause. However, since the CDPS and LLBL regions are involved, as opposed to the LLBL and magnetosheath regions, the spatial position of these open field lines must be significantly inside the magnetopause.

The second test is an examination of the possible origin of the low-energy component in the "plasma sheet." For this test a similar reconstruction method was used. Plate 6 shows the cold component is a permanent feature of the "plasma sheet" where four sample distributions from the different "plasma sheet" regions as identified by the bulk parameters in Plate 3 are presented. Even though the total period covered in the above sample is about 3.5 hours, the cold ion component is seen to be present in all four distributions, and is associated with low energy electrons which have a parallel temperature anisotropy.

We then took a representative "plasma sheet" ion distribution (specifically, an average between 1800:31 and 1805:35 UT) and removed the low-energy component by making the distribution flat at speeds less than 1000 km s^{-1}. To this flattened distribution we added different percentages of the CDPS distribution observed at 1914 UT. The results of this superposition are shown in the bottom row of Figure 7. We repeated the process for the electrons, but flattened the electron distribution at velocities below 18,000 km s^{-1}. The resultant electron distributions are shown in the top two rows of Figure 7.

As can be seen, the initial electron distribution, as well as those in Plate 6, can be reproduced by this superposition of distributions with between 5% an 10% of the CDPS population added to the high-energy component seen in the "plasma sheet." For the ions a slightly higher percentage between 10% and 20% has to be added.

The fraction needed to make up the low energy component is consistent with the fraction determined from the bulk parameters in Plate 3. The higher percentage required for the ions could possibly be due to the electrons having a higher loss rate with their higher speed or mobility along the field lines and their precipitation into the ionosphere. Alternatively, the ratios may be different due to local heating or loss processes which

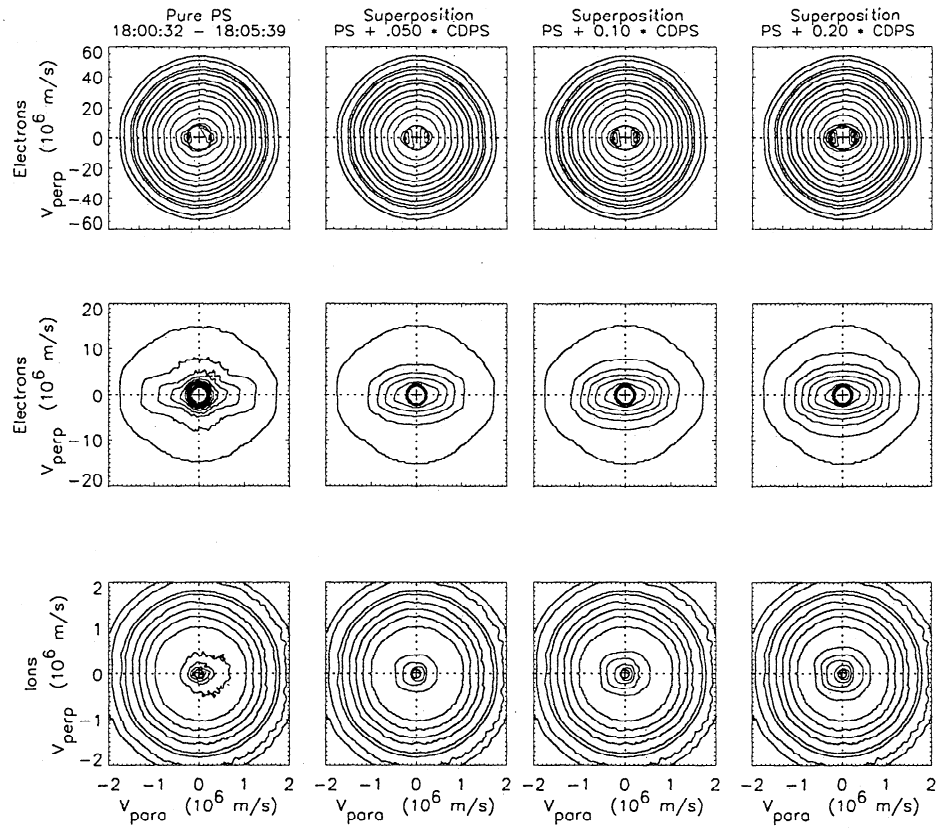

Figure 7. Reconstruction of the plasma sheet populations in Plate 6 using the plasmas sheet populations with no cold present and adding CDPS populations at the given percentages. The cold component seen in the plasma sheet is consistent with the presence of cold magnetosheath plasma deep within the magnetosphere.

are not taken into account by a simple superposition. In either case the cold component is consistent with the presence of plasma of magnetosheath origin. The hot or energetic component appears to have a different origin and history within the magnetosphere since its properties are anticorrelated with the magnetosheath component.

7. Multifluid Simulations

An understanding of the above can be developed through the use of global multifluid simulations where the flow of the ionospheric plasma and solar wind plasma into the magnetosphere are tracked separately. The model is the same as used by *Winglee* [1998a,b] to identify the position of the geopause. Specifically for the electrons, it is assumed that they have sufficiently high mobility along the field lines so that they are approximately in steady state or drift motion ($d\boldsymbol{V}/dt = 0$), so that the electron momentum equation reduces to

$$\boldsymbol{E} + \frac{\boldsymbol{V}_e \times \boldsymbol{B}}{\boldsymbol{c}} + \frac{\nabla P_e}{en_e} = 0\ . \tag{1}$$

Equation (1) is equivalent to the modified Ohm's law with Hall and grad P corrections included. The rest of the electron dynamics are given by assuming quasi-neutrality, and applying the definitions for current, and electron pressure, that is,

$$n_e = \sum_i n_i, \quad \boldsymbol{V}_e = \sum_i \frac{n_i}{n_e}\boldsymbol{V}_i - \frac{\boldsymbol{J}}{en_e}, \quad \boldsymbol{J} = \frac{c}{4\pi}\nabla \times \boldsymbol{B} \tag{2}$$

$$\frac{\partial P_e}{\partial t} = -\gamma\nabla\cdot(P_e\,\boldsymbol{V}_e) + (\gamma-1)\,\boldsymbol{V}_e\cdot\nabla P_e\ . \tag{3}$$

The ion dynamics are attained by substituting the modified Ohm's law (1) for the electric field in the ion momentum equation, which gives

$$\rho_\alpha \frac{dV_{\|\alpha}}{dt} = -(\nabla P_\alpha)_\| - \frac{n_\alpha}{n_e}(\nabla P_e)_\|\ , \tag{4}$$

$$\begin{aligned}\rho_\alpha \frac{dV_{\perp\alpha}}{dt} &= en_\alpha\Big(\frac{V_\alpha \times B}{c} - \sum_i \frac{n_i}{n_e}\frac{V_i \times B}{c}\Big) \\ &+ \frac{n_\alpha}{n_e}\Big(\frac{J\times B}{c} - (\nabla P_e)_\perp\Big) - (\nabla P_\alpha)_\perp,\end{aligned} \tag{5}$$

where the $\|$ and $\perp$ subscripts indicate components parallel and perpendicular to the magnetic field, respectively. For a plasma with a single ion component, (5) reduces to the MHD momentum equation.

To remove high-frequency cyclotron oscillations, the different ion species are assumed to have the same drifts across the magnetic field, that is,

$$\boldsymbol{V}_\perp = \sum_i \rho_i \boldsymbol{V}_{i,\perp} / \sum_i \rho_i \ . \quad (6)$$

This approximation is the same as assumed in MHD, and is equivalent to assuming that the convective drifts are much larger than the gradient B drifts. For the calculated bulk temperatures (< 10 keV), this assumption is true for the majority of the plasma, but the particles in the tail of the distribution can have significant gradient B drifts, particularly in the inner magnetosphere. Assuming (6) the velocity of the perpendicular ion flow is given by

$$\sum_\alpha \rho_\alpha \frac{dV_{\perp\alpha}}{dt} = \left(\frac{J \times B}{c} - (\nabla P_e)_\perp\right) - \sum_\alpha (\nabla P_\alpha)_\perp \ , \quad (7)$$

where

$$\frac{\partial P_\alpha}{\partial t} = -\gamma \nabla \cdot (P_\alpha \boldsymbol{V}_\alpha) + (\gamma - 1)\, \boldsymbol{V}_\alpha \cdot \nabla P_\alpha \ . \quad (8)$$

The above equations are solved using a two-step Lax-Wendroff differencing scheme [*Richtmyer and Morton*, 1967] with Lapidus smoothing on plasma properties only. The latter is required to remove unphysical grid point oscillations across sharp discontinuities such as the bow shock. A high grid resolution of 0.3 R_E is used in the near-Earth region around Wind for $-6 < x < -30\ R_E$, $-3 < y < 20\ R_E$, and $-7.5 < z < 5\ R_E$ GSM system. The grid spacing then increases as one moves outward, to 0.6 R_E in the dayside and midtail regions, and to about 3 R_E in the distant tail at $x \simeq 200 R_e$ and at the flanks at $\pm 60 R_E$.

The inner radius of the simulations is set to 3 R_E. A plasma with a density of 400 cm^{-3} is placed around the inner radius. This plasma represents the plasmaspheric/ionospheric source. The initial profile is assumed to decrease as R^{-6}. Owing to the interaction with the solar wind, the plasma profile can be distorted from this initial profile, but the inner boundary density is held fixed. The plasma that goes to form the magnetosphere must either come from this low-altitude (ionospheric) source or from the solar wind source.

The simulations are first run for 2 hours real time with the solar wind conditions at 1700 UT to establish a magnetosphere in approximate equilibrium. The observed solar conditions are then used to drive the system.

In order to show the position of the Wind spacecraft relative to the plasma sheet, the top panels in Plate 7 show cross-tail cuts in the total plasma pressure as view from the tail. The right-hand panels show a close up of the region near Wind. The overall configuration seen in the total pressure plot is very similar to that in MHD simulations, where the high-pressure regions representing the magnetosheath and plasma sheet form a theta, with the two low-pressure regions representing the northern and southern lobes. The classical picture from MHD is that the region interior to the magnetopause is the LLBL, and that interior to this region is the plasma sheet.

The multifluid treatment shows that this classical picture is oversimplified because there is substantial mixing of the plasmas from the solar wind and ionosphere over key regions within the magnetosphere that are well away from the magnetopause. To show the extent of the mixing region, the lower panels of Plate 8 show the relative contributions from the solar wind and ionospheric sources to the total plasma pressure. Regions with a relative pressure > 50% are supported primarily by ionospheric plasma, while regions where the relative pressure is below 50% are primarily supported by the solar wind plasma. It is seen that at the location of Wind at 1700 UT the total plasma pressure is supported by almost equal amounts of solar wind and ionospheric plasmas. In other words, the Wind position at this time corresponds to the pressure geopause [cf. *Winglee*, 1998a] and is several R_E from the magnetopause.

The corresponding density profiles are shown in Plate 8. Owing to the predominantly positive IMF B_y, there is preferential penetration of the solar wind plasma from the dawnside of the plasma sheet. This plasma is seen in the simulations to be relatively cold, with a temperature of about 80 eV. This cold plasma is able to penetrate several R_E from the magnetopause and is, in fact, the dominant contribution to the density dawn current sheet as seen in Plate 8c. The density from the ionospheric source is at a local maximum in the vicinity of Wind. The plasma also tends to be hotter than the magnetosheath plasma, with a temperature of about 200 eV. The density of these components is approximately equal in the vicinity of Wind at this time, indicating that the spacecraft is also near the density geopause, which would account for the approximately equal amounts of low- and high-energy plasma seen by Wind. In addition, the density of the energetic (ionospheric) component seen in the model decreases toward the magnetopause, and the cold (magnetosheath) component increases, consistent with the Wind observations.

Another feature in the density profiles that is consistent with the Wind data is that the density of cold plasma in the Northern Hemisphere near Wind is substantially enhanced over that seen in the Southern Hemisphere. This asymmetry can account for the fact that Wind sees the highest densities on crossing from the southern current sheet (negative B_x) to the northern current sheet (positive B_x).

This differential penetration of sheath plasma in the northern dawn sector is due to the high dipole tilt (> 20°) where the Northern Hemisphere is pointed to the Sun and to the presence of a relatively strong duskward component in the IMF. As such, the solar

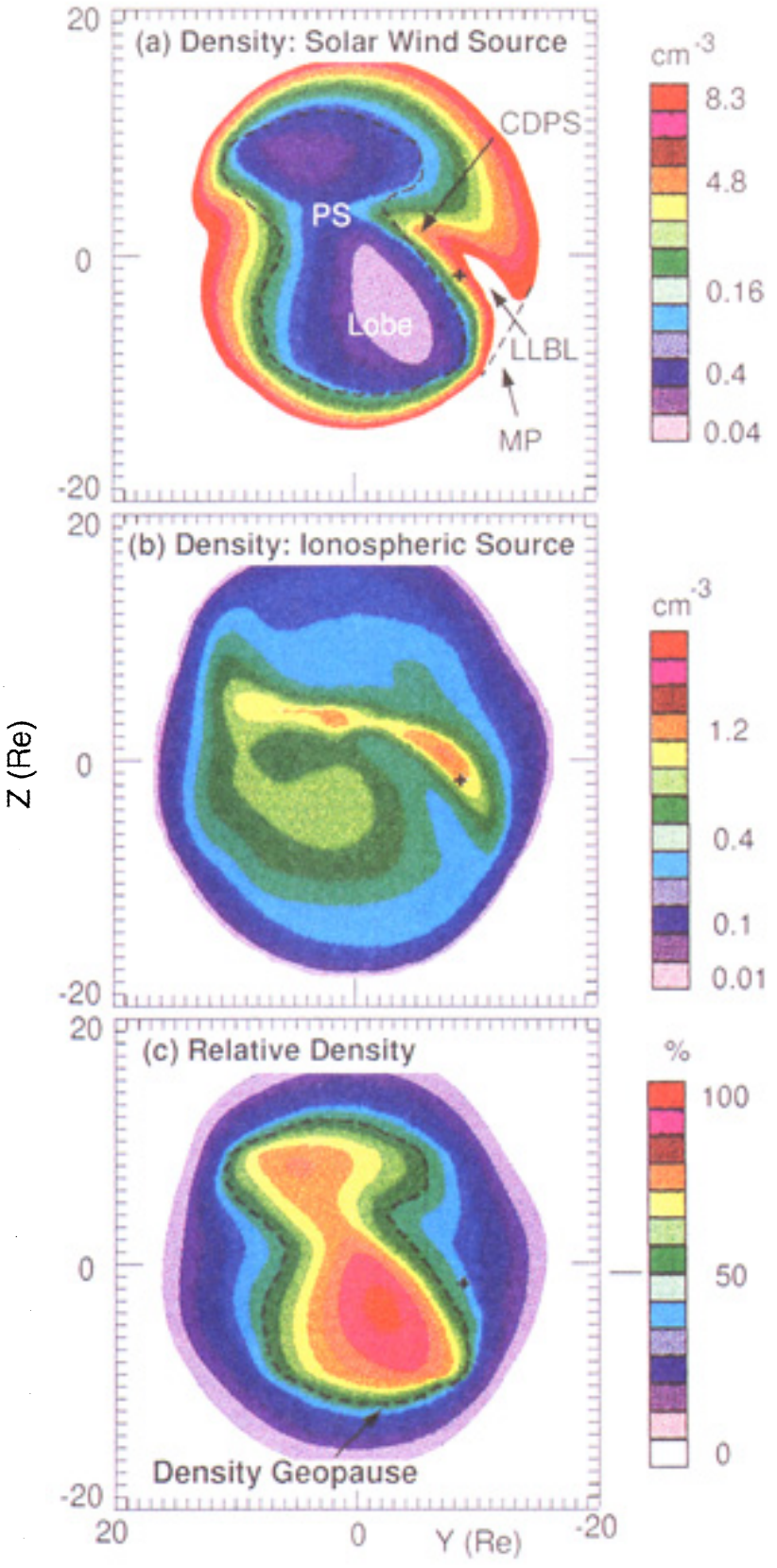

Plate 8. The relative contributions to density at 1700 UT. The ionospheric source dominates the central regions of the current sheet, with Wind at this time being near the density geopause, consistent with the Wind data showing equal densities of cold, magnetosheath-like plasma and hot plasma. In addition, the results show preferential penetration of sheath plasma in the northern-dawn sector of the current sheet and show that this plasma can penetrate deep into the magnetosphere, albeit at reduced densities.

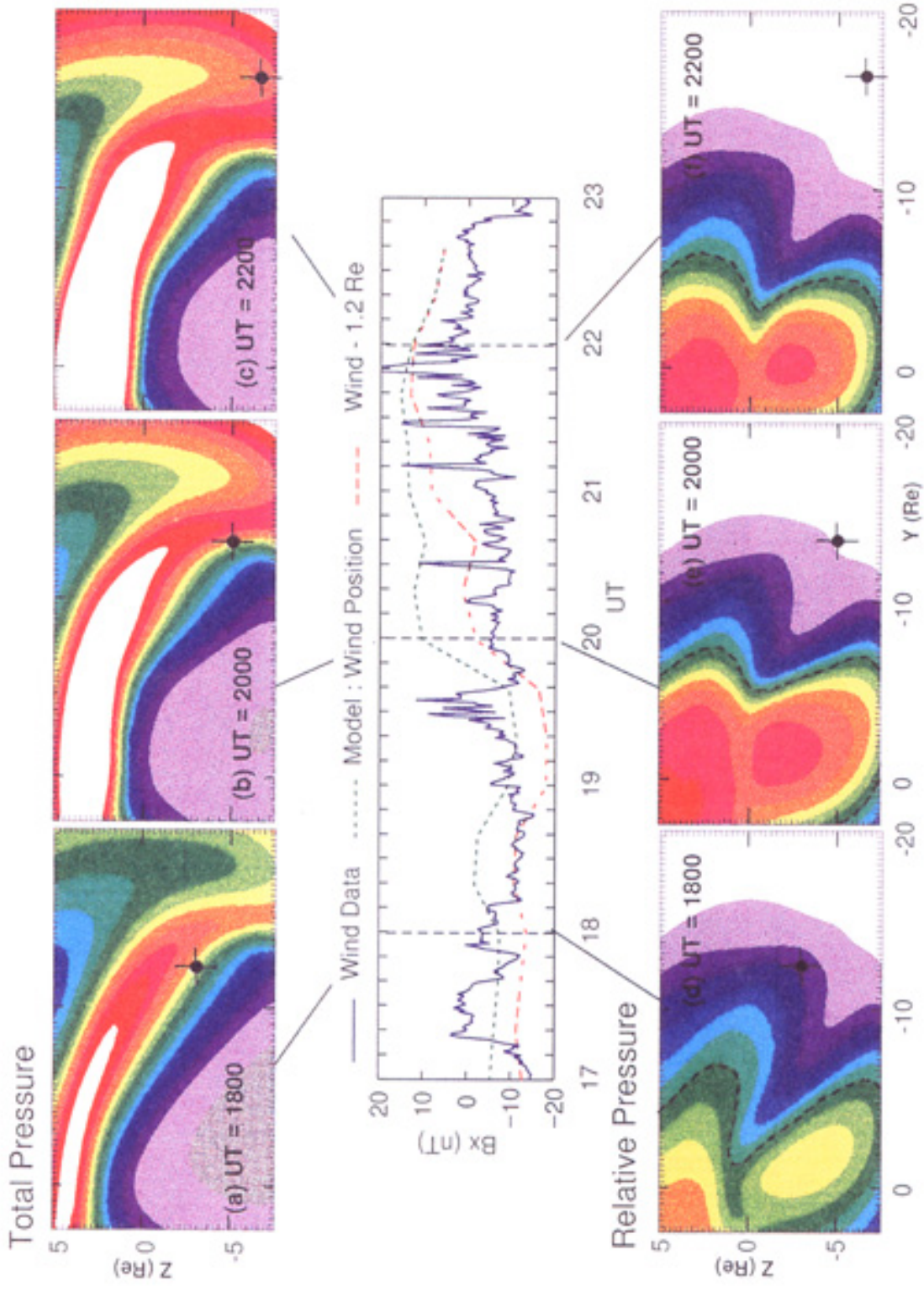

Plate 9. Snapshots of the total and relative pressures. The middle graphs show B_x as observed by Wind (solid line) and the dashed lines the values determined from the model at Wind and at a position displaced 1.2 R_E. Owing to the close proximity of Wind to the center of the current sheet, substantial variations in B_x are seen. The variations in the Wind data can be accounted for in the model by shifts in the current sheet by about 1 R_E.

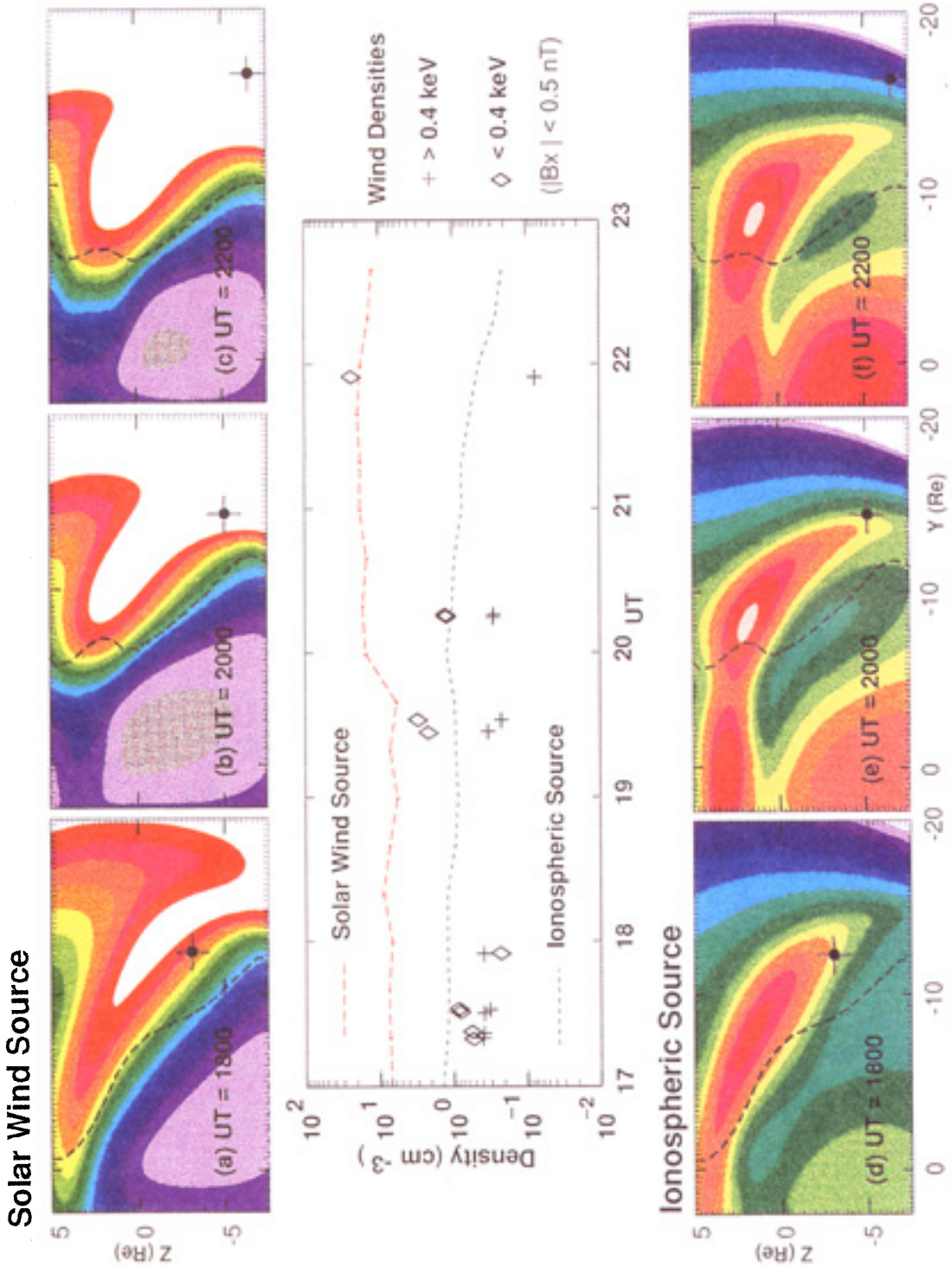

Plate 10. Evolution of the density from the solar wind and ionospheric densities. The solar wind source increases near the magnetopause, particularly in the Northern Hemisphere, but penetration into the middle of the magnetosphere is limited due to IMF B_z being more southerly at later times. Enhanced ionospheric outflow is also seen, with the density of the ionospheric source mostly closely tracking the high-energy component seen in the Wind data. The density of the solar wind source tracks the low-energy component but overpredicts the density by a factor of nearly 4. Part of the discrepancy may be due to the 80 eV cutoff in the Wind data.

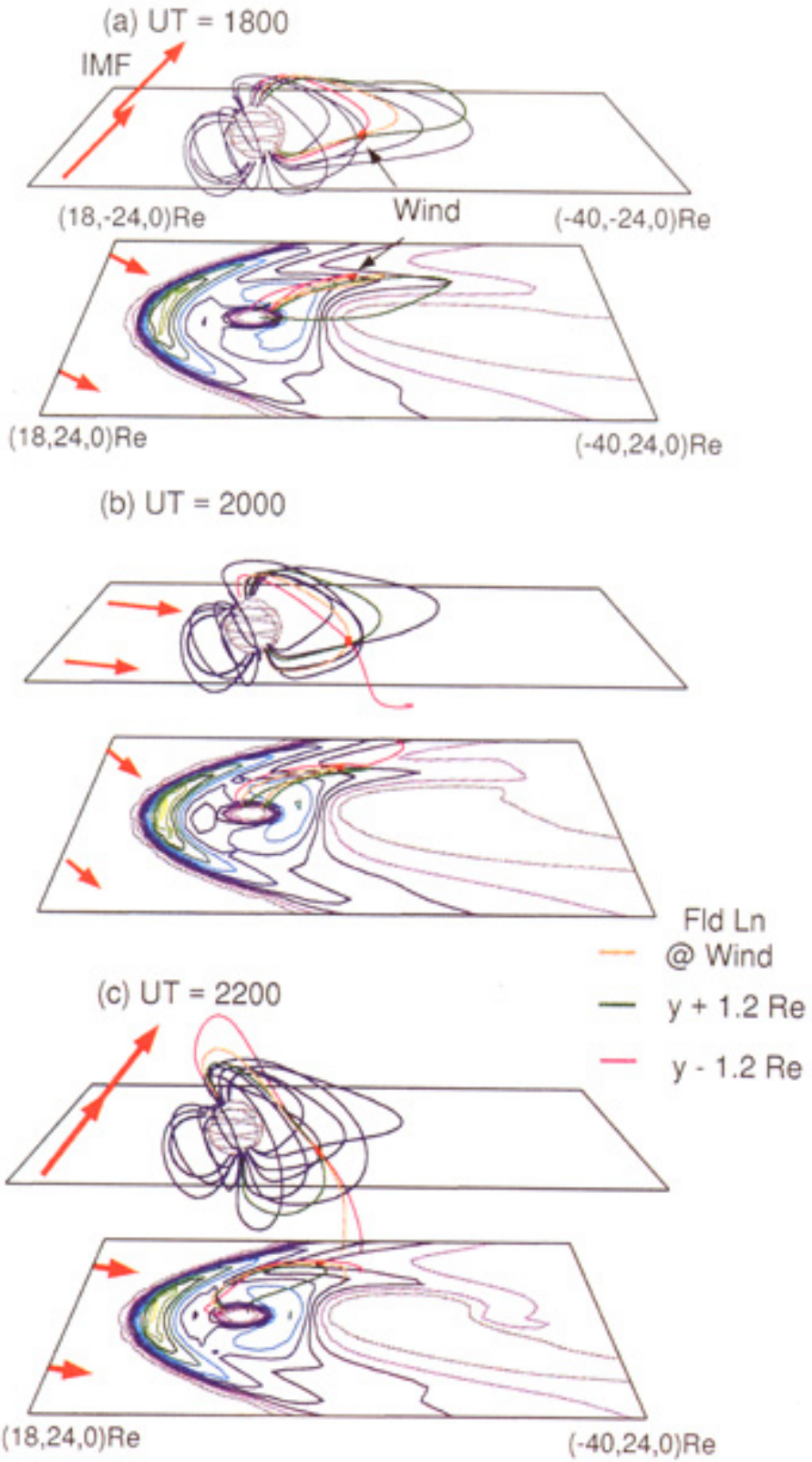

Plate 11. Mapping of the field lines derived from the model. Different positions at $\pm 1.2\, R_E$ are given to show possible variations due to model uncertainties. The model indicates that Wind should be on closed field lines for much of the event, except as the magnetopause is approached when open field lines are encountered before attaining the magnetosheath proper, consistent with the observed particle distributions. The presence of magnetosheath plasma at Wind required entry via open field lines and its subsequent closing of these field lines as they convect into the magnetosphere.

wind plasma has easier direct entry into the Northern Hemisphere. Due to the duskward IMF, reconnection tends to occur on the dusk flank, and the newly reconnected field line, which is attached to the Northern Hemisphere, is draped over the north dawn sector in the tail, leading to preferential magnetosheath mass in this region. On the other hand the Southern Hemisphere (including the southern cusp) is in the wake of the Earth so that the solar wind plasma has less access to the region. As such, the ionospheric plasma is preferentially drawn outward leading to preferential ionospheric mass loading of the southern (winter) hemispheric section of the tail.

As noted by *Winglee* [1998a,b], the position of the geopause is very sensitive to the solar wind conditions. The evolution of the pressure geopause is illustrated in Plate 9. The top panels show the total plasma pressure with the high-pressure regions representing the plasma sheet, while the bottom panels show the relative pressure with the dashed line indicating the pressure geopause. During the event, the plasma sheet pressure is seen to increase on average. This increase is correlated with the increase in the dynamic pressure of the solar wind as seen in Figures 2 and 5. At the same time the pressure geopause is seen to retreat away from the magnetopause [cf. *Winglee*, 1998a,b].

The origin of some of the variations seen in the Wind data can be identified in the middle panels which shows B_x as observed by Wind (blue line), as derived by the model at the nominal Wind position (green dashed line), and at a position shifted by 1.2 R_E toward the dusk (red dashed line). The size of this 1.2 R_E shift relative to the size of the current sheet is indicated by the lines drawn through the point representing the Wind spacecraft position. It is seen that even with just a 1.2 R_E shift in position, a substantial change in the observed B_x is produced due to the proximity of the spacecraft to the center of the current sheet. In particular, the model at the nominal Wind position predicts that it crosses the current sheet probably an hour too early. The shift of 1.2 R_E is seen to give a better fit to the observations. Note that the observed fields lie essentially between the two curves so that the motion of the current sheet produced by the solar wind pressure pulses could be accounted for by shifts in the sheet position by about an R_E.

The corresponding changes in the density contributions from the solar wind and ionospheric sources are shown in Plate 10. The enhanced intrusion of cold plasma from the magnetosheath is clearly seen in the top panels. In addition, though, there is also enhanced ionospheric plasma flowing into the tail causing the density geopause to actually move closer to a magnetopause as indicated by the dashed lines in top and bottom panels. Despite this motion it is seen on comparing Plates 7 and 9 that the density geopause lies closest to the spacecraft at 1700 UT.

The middle panel of Plate 10 displays the evolution of the two density components at the nominal Wind position. The density of the ionospheric component shows the same trend as the high-energy component seen by Wind, decreasing as the magnetopause is approached. The model results differ in that they are typically a factor of 2 higher.

The density of the magnetosheath component agrees well with the low-energy component seen by Wind, particularly after 1900 UT. An important discrepancy between the model results and Wind is that the model overpredicts the presence of cold plasma between 1700 and 1900 UT. There are two possible explanations for this discrepancy. The first is that the Wind instrument only measures ions to down to 80 eV, whereas the model results indicate that the plasma temperature is only about 60 eV in this region. In this case the Wind instrument would not observe a significant fraction of the distribution present. An alternate explanation is that the fluid description assumes Maxwellian distributions which are only adiabatically heated, whereas the actual particles may undergo strong wave-particle heating as the two populations interact. Such heating might produce the same total plasma pressure with fewer particles. This discrepancy can only be resolved with particle measurements at lower energies and full particle models.

The presence of significant amounts of magnetosheath-like plasma on a magnetospheric field line is sometimes used as evidence that the field line is open. In order to test this hypothesis, the field line mapping the vicinity of Wind is displayed in Plate 11. In each panel, closed field lines are shown in purple while the instantaneous field line through Wind is shown in orange. For estimates of potential errors, field lines $\Delta y = \pm 1.2\ R_E$ are shown in green and magenta. Projections of these field lines into the equatorial plane are shown superimposed on contours of the total plasma pressure in the bottom section of each panel. The instantaneous direction of the IMF is indicated by the red arrows. It is seen that at both the nominal Wind position and $\Delta y = +1.2\ R_E$ (which gave the better fit for the observed magnetic field) the field lines are closed until the magnetopause is approached at 2200 UT. This result is consistent with the symmetric ion and electron distributions observed by Wind until the MSBL, which is seen shortly before the magnetopause crossing at 2200 UT.

8. Summary and Conclusions

The evolution of the different plasma populations within the current sheet has been investigated using observations from the Wind 3-D plasma and energetic particle experiment during the perigee pass of May 10, 1996. During this pass the Wind spacecraft makes several current sheet crossings that enable the evolution of the current sheet populations to be evaluated as a func-

tion of axial distance from the magnetopause without ambiguities introduced by the z distance from the center of the current sheet. The data were then compared with the structure of the tail determined from multifluid simulations which are able to identify the sources (either ionospheric or solar wind) that compose the key regions of the magnetosphere. The evolution derived from the simulations appears to give a natural explanation of the observed evolution with the main conclusions being the following:

1. The low-energy ion density at the center of the current sheet increases smoothly with radial distance and is probably of magnetosheath origin. The high-energy component decreases monotonically, indicating that it has a different source, presumably the ionosphere, or that the particles are undergoing energization near the noon-midnight meridian. The crossover point where the densities of these two components are approximately equal could well represent the geopause and lies about 5 R_e from the magnetopause in the present study.

2. Owing to pressure pulses in the solar wind, Wind was able to sample the plasma on opposite sides of the current sheet several times during the pass. The data show an asymmetry between Northern and Southern Hemispheres, with higher densities being present in the Northern Hemisphere. This asymmetry is also seen in the model and appears to be due to the high dipole tilt that was present during the event.

3. The cold, dense plasma sheet as identified by *Fujimoto et al.* [1998a,b] is seen to penetrate deep into the magnetosphere (at least 5 R_e from the magnetopause) and is likely to be of magnetosheath origin.

4. Bidirectional electron distributions which have often been considered evidence for closed field lines appear to be correlated with the entry of cold, magnetosheath-like plasma. The magnetic field mapping derived from the modeling is consistent with this picture.

5. The modeling also shows that the cold magnetosheath-like plasma can penetrate well beyond the 5 R_e attributed to the CDPS, so that the actual plasma sheet is invariably a mixture of ionospheric plasma and the magnetosheath plasma. The more energetic particles in the tail appear in the model to be produced near the noon-midnight meridian (and of seemingly ionospheric origin), and this spatial dependence can account for the anticorrelation of the energetic particles with the cold, magnetosheath-like plasma seen in the observations.

6. The magnetosheath-like plasma that is observed deep within the magnetosphere is seen to have in most cases a symmetric distribution, indicating that these plasma components are on possibly closed field lines but distributions which have flow asymmetries similar to those reported for the MSBL are also seen; however, in the present case the flow appears to be between the LLBL and CDPS. The modeling shows that the entering magnetosheath plasma can be on closed field lines. The entry process is thereby produced by high-latitude reconnection and the subsequent convection of the plasma into the magnetosphere [cf. *Winglee*, 1998a,b].

7. Motions of the geopause need not be correlated with those of the magnetopause so that changes in the relative plasma populations should not be taken to indicate proximity to the magnetopause.

Acknowledgment. This work was supported by NSF Grant ATM-9731951 and by NASA grants NAG5-6244 and NAG5-8089 to the University of Washington. The simulations were supported by the Cray T-90 at the San Diego Supercomputing Center which is supported by NSF. The authors wish to thank R. Lepping for the use of the magnetic field data.

Janet G. Luhmann thanks O. Walter Lennartsson and Steve A. Fuselier for their assistance in evaluating this paper.

References

Borovsky, J. E., M. F. Thomsen, and D. J. McComas, The superdense plasma sheet: Plasmaspheric origin, solar wind origin, or ionospheric origin?, *J. Geophys. Res.,102*, 22,089, 1997.

Chappell, C. R., T. E. Moore, and J. H. Waite Jr., The ionosphere as a fully adequate source of the Earth's magnetosphere, *J. Geophys. Res., 92*, 5896, 1987.

Delcourt, D. C, C. R. Chappell, T. E. Moore, and J. H. Waite Jr., A three-dimensional numerical model of ionospheric plasma in the magnetosphere, *J. Geophys. Res., 94*, 11,893, 1989.

Delcourt, D. C, J. A. Sauvaud, and T. E. Moore, Polar wind ion dynamics in the magnetotail, *J. Geophys. Res., 98*, 9155, 1993.

Elsen, R. K., and R. M. Winglee, The average shape of the magnetopause: A comparison of three-dimensional global MHD and empirical models, *J. Geophys. Res., 102*, 4799, 1997.

Fujimoto, M., T. Terasawa, and T. Mukai, Structure of the low-latitude boundary layer: A case study with Geotail data, *J. Geophys. Res., 103,* 2297, 1998a.

Fujimoto, M., T. Terasawa, and T. Mukai, Plasma entry from the flanks of the near-Earth magnetopause: Geotail observations, *J. Geophys. Res., 103,* 4391, 1998b.

Fuselier, S. A., B. J. Anderson, and T. G. Onsager, Electron and ion signatures of field line topology at the low-shear magnetopause, *J. Geophys. Res., 102,* 4847, 1997.

Lennartsson, W., Plasma sheet ion composition at various levels of geomagnetic and solar activity, *Phys. Scripta, 36*, 367, 1987.

Lennartsson, W., A scenario for solar wind penetration of Earth's magnetic tail based on ion composition data from the ISEE 1 spacecraft, *J. Geophys. Res., 97*, 19221, 1992.

Lepping, R. P., et al., The Wind magnetic field investigation, *Space Sci. Rev., 71*, 207, 1995.

Lin, R. P., et al., A three-dimensional plasma and energetic particle investigation for the Wind spacecraft, *Space Sci. Rev., 71*, 125, 1995.

Moore, T. E., Origins of magnetospheric plasma, *Rev. Geophys., 29*, 1039, 1991.

Moore, T. E., and D. C. Delcourt, The geopause, *Rev. Geophys., 33*, 175, 1995.

Paschmann, G., Observational evidence for transfer of plasma across the magnetopause, *Space Sci. Rev., 80*, 217, 1997.

Paschmann, G., et al., Plasma acceleration at the Earth's magnetopause: Evidence for reconnection, *Nature, 282*, 243, 1979.

Phan, T. D., et al., Low-latitude dusk flank magnetosheath, magnetopause. and boundary layer for low magnetic shear: Wind observations, *J. Geophys. Res., 102,* 19,883, 1997.

Richtmyer, R. D., and K. W. Morton, *Difference Methods for Initial Value Problems*, p. 300, Wiley-Interscience, New York, 1967.

Roelof, E. C., and D. G. Sibeck, Magnetopause shape as a bivariate function of interplanetary magnetic field B_z and solar wind dynamic pressure, *J. Geophys. Res., 98,* 21,421, 1993.

Sckopke, N., G. Paschmann, G. Haerendel, B. U. O. Sonnerup, S.J. Bame, T. G. Forbes, E. W. Hones Jr., and C. T. Russell, Structure of the low-latitude boundary layer, *J. Geophys. Res., 86*, 2099, 1981.

Song, P., R. C. Elphic, C. T. Russell, J. T. Gosling, and C. A. Cattell, Structure and properties of the subsolar magnetopause for northward IMF: ISEE observations *J. Geophys. Res., 95*, 6375, 1990.

Song, P., C. T. Russell, R. J. Fitzenreiter, J. T. Gosling, M. F. Thomsen D. G. Mitchell, S. A. Fuselier, G. K. Parks, R. R. Anderson, and D. Hubert, Structure and properties of subsolar magnetopause for northward interplanctary magnetic field: Multi-instrument particle observations, *J. Geophys. Res., 98,* 11,319, 1993.

Terasawa, T., M. Fujimoto, T. Mukai, I. Shinohara, Y. Saito, T. Yamamoto, S. Machida, S. Kokubun, A. J. Lazarus, J. T. Steinberg, and R. P. Lepping, Solar wind control of density and temperature in the near-Earth plasma sheet: Wind/Geotail collaboration, *Geophys. Res. Lett., 24*, 935, 1997.

Williams, D. J., D. G. Mitchell, T. E. Eastman, and L. A. Frank, Energetic particle observations in the low-latitude boundary layer, *J. Geophys. Res., 90*, 5097, 1985.

Winglee, R. M., Multi-fluid simulations of the magnetosphere: The identification of the geopause and its variation with IMF, *Geophys. Res. Lett., 25*, 4441, 1998a.

Winglee, R. M., Imaging the ionospheric and solar wind sources in the magnetosphere through multi-fluid global simulations, *Phys. Space Plasmas, 15*, 345, 1998b.

L. Chen, Q. Li, G. Parks, M. Wilber, and R. M. Winglee, Geophysics Program, Box 351650, University of Washington, Seattle, WA 98195-1650

(Received May 21, 1999; revised August 13, 1999; accepted August 16, 1999.)